



OPEN ACCESS

EDITED BY

Bradley J. Turner,
University of Melbourne, Australia

REVIEWED BY

Adrian Rodriguez-Contreras,
Northwestern University, United States
Alberto Catanese,
University of Ulm, Germany

*CORRESPONDENCE

Franca Codazzi
✉ codazzi.franca@hsr.it

RECEIVED 05 July 2023

ACCEPTED 13 October 2023

PUBLISHED 13 November 2023

CITATION

Pisciottani A, Croci L, Lauria F, Marullo C, Savino E, Ambrosi A, Podini P, Marchioretto M, Casoni F, Cremona O, Taverna S, Quattrini A, Cioni J-M, Viero G, Codazzi F and Consalez GG (2023) Neuronal models of TDP-43 proteinopathy display reduced axonal translation, increased oxidative stress, and defective exocytosis. *Front. Cell. Neurosci.* 17:1253543. doi: 10.3389/fncel.2023.1253543

COPYRIGHT

© 2023 Pisciottani, Croci, Lauria, Marullo, Savino, Ambrosi, Podini, Marchioretto, Casoni, Cremona, Taverna, Quattrini, Cioni, Viero, Codazzi and Consalez. This is an open-access article distributed under the terms of the [Creative Commons Attribution License \(CC BY\)](https://creativecommons.org/licenses/by/4.0/). The use, distribution or reproduction in other forums is permitted, provided the original author(s) and the copyright owner(s) are credited and that the original publication in this journal is cited, in accordance with accepted academic practice. No use, distribution or reproduction is permitted which does not comply with these terms.

Neuronal models of TDP-43 proteinopathy display reduced axonal translation, increased oxidative stress, and defective exocytosis

Alessandra Pisciottani^{1,2}, Laura Croci², Fabio Lauria³, Chiara Marullo^{1,2}, Elisa Savino², Alessandro Ambrosi^{1,2}, Paola Podini², Marta Marchioretto³, Filippo Casoni^{1,2}, Ottavio Cremona¹, Stefano Taverna², Angelo Quattrini², Jean-Michel Cioni², Gabriella Viero³, Franca Codazzi^{1,2*} and G. Giacomo Consalez^{1,2}

¹Faculty of Medicine and Surgery, Università Vita-Salute San Raffaele, Milan, Italy, ²Division of Neuroscience, IRCCS San Raffaele Scientific Institute, Milan, Italy, ³Institute of Biophysics, CNR Unit at Trento, Povo, Italy

Amyotrophic lateral sclerosis (ALS) is a progressive, lethal neurodegenerative disease mostly affecting people around 50–60 years of age. TDP-43, an RNA-binding protein involved in pre-mRNA splicing and controlling mRNA stability and translation, forms neuronal cytoplasmic inclusions in an overwhelming majority of ALS patients, a phenomenon referred to as TDP-43 proteinopathy. These cytoplasmic aggregates disrupt mRNA transport and localization. The axon, like dendrites, is a site of mRNA translation, permitting the local synthesis of selected proteins. This is especially relevant in upper and lower motor neurons, whose axon spans long distances, likely accentuating their susceptibility to ALS-related noxae. In this work we have generated and characterized two cellular models, consisting of virtually pure populations of primary mouse cortical neurons expressing a human TDP-43 fusion protein, wt or carrying an ALS mutation. Both forms facilitate cytoplasmic aggregate formation, unlike the corresponding native proteins, giving rise to *bona fide* primary culture models of TDP-43 proteinopathy. Neurons expressing TDP-43 fusion proteins exhibit a global impairment in axonal protein synthesis, an increase in oxidative stress, and defects in presynaptic function and electrical activity. These changes correlate with deregulation of axonal levels of polysome-engaged mRNAs playing relevant roles in the same processes. Our data support the emerging notion that deregulation of mRNA metabolism and of axonal mRNA transport may trigger the dying-back neuropathy that initiates motor neuron degeneration in ALS.

KEYWORDS

amyotrophic lateral sclerosis, TDP-43 proteinopathy, cortical neurons, axonal translation, oxidative stress, synaptic function, calcium, polysome profiling

Introduction

Amyotrophic lateral sclerosis (ALS) is a progressive, lethal neurodegenerative disease affecting people around 50–60 years of age. The most common clinical signs are muscular weakness, spasticity, fasciculations and dysphagia, culminating in progressive paralysis and death (reviewed in [Brown and Al-Chalabi, 2017](#); [Hardiman et al., 2017](#)). The most frequent cause of death is respiratory failure (reviewed in [Gil et al., 2008](#); [Niedermeyer et al., 2019](#)). About 10% of ALS patients also show cognitive impairment consistent with fronto-temporal dementia (FTD), which is characterized by degeneration of neurons of the frontal and temporal lobes. More broadly, up to 50% of patients develop cognitive and/or behavioral impairments during disease progression (reviewed in [Brown and Al-Chalabi, 2017](#)). Ten percent of ALS cases show familial inheritance, while the majority of patients have no family history and are classified as sporadic cases (reviewed in [Hardiman et al., 2017](#)). ALS neuropathology is characterized by the degeneration of upper (cortical) and lower (cranial and spinal) motor neurons.

Since 1994, many ALS causative genes and risk factors have been discovered, including a number of genes primarily involved in RNA metabolism. The involvement of RNA-binding proteins (RBPs; [Sreedharan et al., 2008](#); [Blair et al., 2010](#)) highlights the importance of altered RNA processing in ALS. TDP-43, a ubiquitously expressed RBP, has several functions: pre-mRNA splicing ([Buratti et al., 2001](#); [Polymenidou et al., 2011](#); [Tollervey et al., 2011](#); [Fratta et al., 2018](#); [Watanabe et al., 2020](#); [Brown et al., 2022](#)), mRNA stability ([Strong et al., 2007](#); [Colombrita et al., 2012](#); [Costessi et al., 2014](#)), including that of its own transcript ([Ayala et al., 2011](#)), mRNA transport ([Alami et al., 2014](#); [Nagano et al., 2020](#)), and the control of mRNA translation ([Chu et al., 2019](#); [Briese et al., 2020](#); [Lauria and Maniscalco, under revision](#)). TDP-43 is encoded by *TARDBP*, whose mutations account for about 5%–10% of all forms of familial ALS ([Sreedharan et al., 2008](#); [Kraemer et al., 2010](#)). However, while *TARDBP* mutations are relatively infrequent in ALS patients, TDP-43 is the main component of neuronal cytoplasmic inclusions found in 97% of all ALS patients, of both sporadic and familial origin. This phenomenon is referred to as TDP-43 proteinopathy ([Arai et al., 2006](#); [Neumann et al., 2006](#)). TDP-43, a predominantly nuclear protein (reviewed in [Cohen et al., 2011](#)), binds UG-rich regions of RNA targets ([Buratti et al., 2001](#); [Ayala et al., 2005](#)), then shuttles to the cytoplasm ([Ayala et al., 2008](#)). Its C-terminal domain contains an intrinsically disordered protein region, the low complexity domain, which promotes liquid–liquid phase separation (LLPS) and liquid droplet formation, leading to the assembly of RNA granules (reviewed in [Harrison and Shorter, 2017](#); [Wolozin and Ivanov, 2019](#)). Interestingly, the majority of ALS-mutations, located in the C-terminal domain (reviewed in [Buratti, 2015](#); [Prasad et al., 2019](#)), modulate the ability of TDP-43 to induce LLPS ([Conicella et al., 2016](#)) and may promote cytoplasmic aggregate formation, disrupting the subcellular transport and localization of its target mRNAs. While many proteins are synthesized in the neuronal soma and transported into the axon by fast or slow axonal transport (reviewed in [Guo et al., 2020](#)), the axon, like dendrites, is a site of local mRNA translation (reviewed in [Jung et al., 2012](#); [Martinez et al., 2019](#); [Shigeoka et al.,](#)

[2019](#); [Fusco et al., 2021](#)). Messenger RNAs are transported along the axon to synthesize selected proteins locally through the translation machinery, whose composition undergoes remodeling *in situ* ([Shigeoka et al., 2019](#); [Fusco et al., 2021](#)). Local translation occurs both constitutively and in response to stimuli acting far away from the cell body, in the axon and presynaptic terminal. Locally synthesized proteins include factors involved in axonal growth ([Lee et al., 2018](#)), axonal viability ([Cosker et al., 2016](#)), and translation ([Fusco et al., 2021](#)). Axonal translation contributes not only to developing or regenerating axons, but also plays a key regulatory and homeostatic role in mature axons ([Shigeoka et al., 2016](#); [Ostroff et al., 2019](#); reviewed in [Kim and Jung, 2020](#)). The axon of upper and lower motor neurons often spans long distances; long axons have an absolute requirement for local response mechanisms largely independent of the cell body – indeed, in a meter-long axon, this compartment accounts for well over 99% of the total neuronal volume (reviewed in [Ragagnin et al., 2019](#)). These features likely accentuate an axon's susceptibility to stressful conditions; indeed, several lines of evidence suggest that ALS is a distal axonopathy, characterized by axonal impairment, which precedes motor neuron degeneration and the onset of clinical signs ([Fischer et al., 2004](#); [Moloney et al., 2014](#)).

The alteration of local mRNA translation in the axon may be a decisive factor in ALS progression, possibly affecting various cellular responses independently of the neuronal soma. For example, oxidative stress is a hallmark of ALS motor neurons, and an increase in reactive oxygen species (ROS) levels and ROS-associated damage have been reported in ALS ([Colombrita et al., 2009](#); reviewed in [Barber and Shaw, 2010](#); [Altman et al., 2021](#); [Lehmkuhl et al., 2021](#); [Wong et al., 2021](#)). While non-cell-autonomous mechanisms play important roles in the pathogenesis of this disorder or in its mitigation (reviewed in [Beers et al., 2006](#); [Marchetto et al., 2008](#); [Wang et al., 2011](#); [Liao et al., 2012](#); [Liu and Wang, 2017](#)), little is known about cell-autonomous signaling events controlling oxidative stress secondary to TDP-43 proteinopathy, and even less about the specific roles played by axons in the response to this condition.

Likewise, synaptic activity may be strictly dependent on local translation in the axon of long-range projection neurons. Indeed, it has been established that mature axons are enriched in transcripts involved in synaptic transmission. Dysregulation of proteins involved in neurotransmitter release have been shown to precede denervation ([Krishnamurthy and Pasinelli, 2021](#)); hence, synaptic dysfunction may be a crucial factor in ALS onset and progression. Excitatory glutamatergic synapses have received special attention in the ALS field ([Genc et al., 2016](#); [Fogarty et al., 2016a,b](#); [Fogarty et al., 2017](#); [Handley et al., 2017](#); [Jiang et al., 2017](#)); however, whereas numerous observations of early postsynaptic spine degeneration have been made, evidence is sparse regarding molecular and functional changes at the presynaptic terminal of corticospinal motor neurons.

Here, we describe a study conducted on homogeneous cultures of mouse cortical neurons (upper motor neurons), expressing a human TDP-43 fusion protein, wt or mutant, which accumulates in the cytoplasm in the form of insoluble aggregates, unlike the corresponding native proteins. This feature allows us to propose our transduced neurons as the first primary culture models of ALS-proteinopathy, characterized by a global impairment in

axonal protein synthesis, an increase in oxidative stress, and defects in presynaptic function and electrical activity.

Results

An *in vitro* model of deep-layer glutamatergic neurons

To investigate the molecular mechanisms involved in the onset and progression of TDP-43 proteinopathy, we developed an *in vitro* model of highly homogeneous murine upper motor neurons (UMNs), i.e., glutamatergic neurons of layers V and VI, amenable to lentiviral transduction with human TDP-43, wild-type (wt) or carrying an ALS-mutation (Gitcho et al., 2008). To obtain primary cortical cultures enriched in glutamatergic neurons of layers V and VI, cells were isolated from the cerebral cortex of mouse embryos harvested at embryonic day 14.5 (E14.5), a developmental stage characterized *in vivo* by a low number of GABAergic neurons and glial cells in the prospective cerebral cortex. Indeed, the immunostaining performed at 3 DIV (Supplementary Figure 1A) revealed that virtually all cells were positive for the neuron-specific β 3-tubulin (Ab: TuJ1), and 97% of them stained double-positive for the T-Box Brain Transcription Factor 1 (TBR1), an early marker of deep-layer glutamatergic neurons (Bedogni et al., 2010). Moreover, about 64% of neuronal cells were double-positive for TuJ1 (neuron-specific type III beta tubulin) and COUP-TF-interacting protein 2 (CTIP2), a transient marker of neurons located in cortical layers V and VI (reviewed in Molyneaux et al., 2007). To quantify the GABAergic component of these cultures, we immunostained these cells for glutamic acid decarboxylase-65 (GAD65). As shown in Supplementary Figure 1B (left), GAD65-positive cells were virtually absent, while they were abundant in neurons harvested at a later developmental stage (E17.5; Supplementary Figure 1B, right). Moreover, the results of EdU incorporation revealed that, while a small number of proliferating progenitors were still present at 2 DIV, all cells lost the ability to replicate DNA at 7 DIV (Supplementary Figure 1C).

Finally, we evaluated the presence of glial cells, which are mostly produced at later stages of cortical development. TuJ1 immunostaining, combined with antibodies against specific glial markers (glial fibrillary acidic protein, GFAP, for astrocytes; oligodendrocyte marker 4, O4, for oligodendrocyte precursors; ionized calcium binding adaptor molecule 1, IBA1, for microglia) revealed the virtual absence of all glial cell types in our mouse UMN cultures (Supplementary Figure 1D, positive controls in Supplementary Figures 1E–G).

In summary, E14.5 cortical neuronal cultures are strongly enriched in postmitotic glutamatergic neurons of deep cortical layers, from which the corticospinal tract arises, and contain a negligible contribution of glial cells or GABAergic neurons.

Cytoplasmic TDP-43 aggregates in wtTDP-43 and mutTDP-43 neurons

A neuronal model of TDP-43 proteinopathy was produced by transducing the above UMN cultures with lentiviral particles to deliver tRFP alone (ctr neurons) or a human tRFP-TDP-43 N-ter fusion protein, either wt or carrying the A315T mutation (henceforth

defined wtTDP-43 and mutTDP-43 neurons, respectively); constructs are sketched in Figure 1A. The transduction efficiency was evaluated using the ArrayScan microscope, as the average percentage of red fluorescent cells over the total cell number (96% for ctr and wtTDP-43 neurons and 97% for mutTDP-43 cells; Figure 1A'). All transduced cells exhibit cytoplasmic aggregates, are viable, and project abundant TuJ1+ neurites (Supplementary Figure 2).

We then assessed the relative expression levels of the exogenous TDP-43 fusion proteins and investigated their subcellular localization, since the cytoplasmic accumulation of TDP-43 is a key feature of ALS neurons (Suk and Rousseaux, 2020). Biochemical analysis, performed on UMN lysates with an antibody recognizing both human and murine TDP-43, detected the expression of total TDP-43 protein (about 4-times higher than the endogenous protein in ctr cells; Figure 1B, solid arrows, quantified in Figure 1B'); notably, the level of endogenous murine TDP-43 is somewhat reduced in wtTDP-43 and mutTDP-43 neurons, probably due to negative post-transcriptional autoregulation (Ayala et al., 2011; Avendano-Vazquez et al., 2012; Figure 1B''). A ~65 kDa band likely represents a degradation product of the fusion protein. Furthermore, a more prolonged exposure of chemiluminescence-stained membranes revealed, both in wtTDP-43 and mutTDP-43 neurons, the presence of TDP-43 proteolytic fragments, a typical hallmark of ALS neurons (Figure 1B, empty arrows; Neumann et al., 2006).

To further characterize TDP-43 expression, we set up a subcellular fractionation protocol to separate nuclear from soluble and insoluble cytosolic fractions (Supplementary Figure 3A). The results of western blotting performed on subcellular lysates display an enrichment of exogenous wtTDP-43 and mutTDP-43 proteins in the insoluble fraction (upper solid arrow; Supplementary Figure 3B); interestingly, 25 kDa degradation products are restricted to the insoluble fraction (empty arrow; Supplementary Figure 3B). The cytoplasmic accumulation of exogenous TDP-43, a key feature of ALS neurons (Suk and Rousseaux, 2020), was confirmed by immunocytochemistry, revealing a predominantly nuclear localization of the endogenous TDP-43 in ctr neurons (Neumann et al., 2006) in contrast with an enrichment of both wtTDP-43 and mutTDP-43 in cytoplasmic aggregates (Figure 1C). Numerous cytoplasmic aggregates are also found in neurites (Figure 1D). Importantly, cytoplasmic localization is not dependent on overexpression, since an overexpressed TDP-43 fused to a shorter tag (see methods) maintains a nuclear distribution (Supplementary Figure 3C).

Our findings are reminiscent of neuronal cytoplasmic aggregates observed in all cortical layers in motor neuron disease with frontotemporal dementia (Mackenzie et al., 2011). Notably, expression of RFP alone does not lead to aggregates; thus, the observed effects are TDP-43-specific. Overall, our results indicate that neurons expressing RFP-TDP-43 fusion proteins recapitulate several key features of TDP-43 proteinopathy within the brief lifespan of a primary neuron culture. To our knowledge, ours is the first *in-vitro* neuronal model of TDP-43 proteinopathy.

Exogenous TDP-43 is recruited to RNA granules

The analysis of tissue samples obtained from 97% of ALS patients has revealed the presence of TDP-43 pathologic inclusions

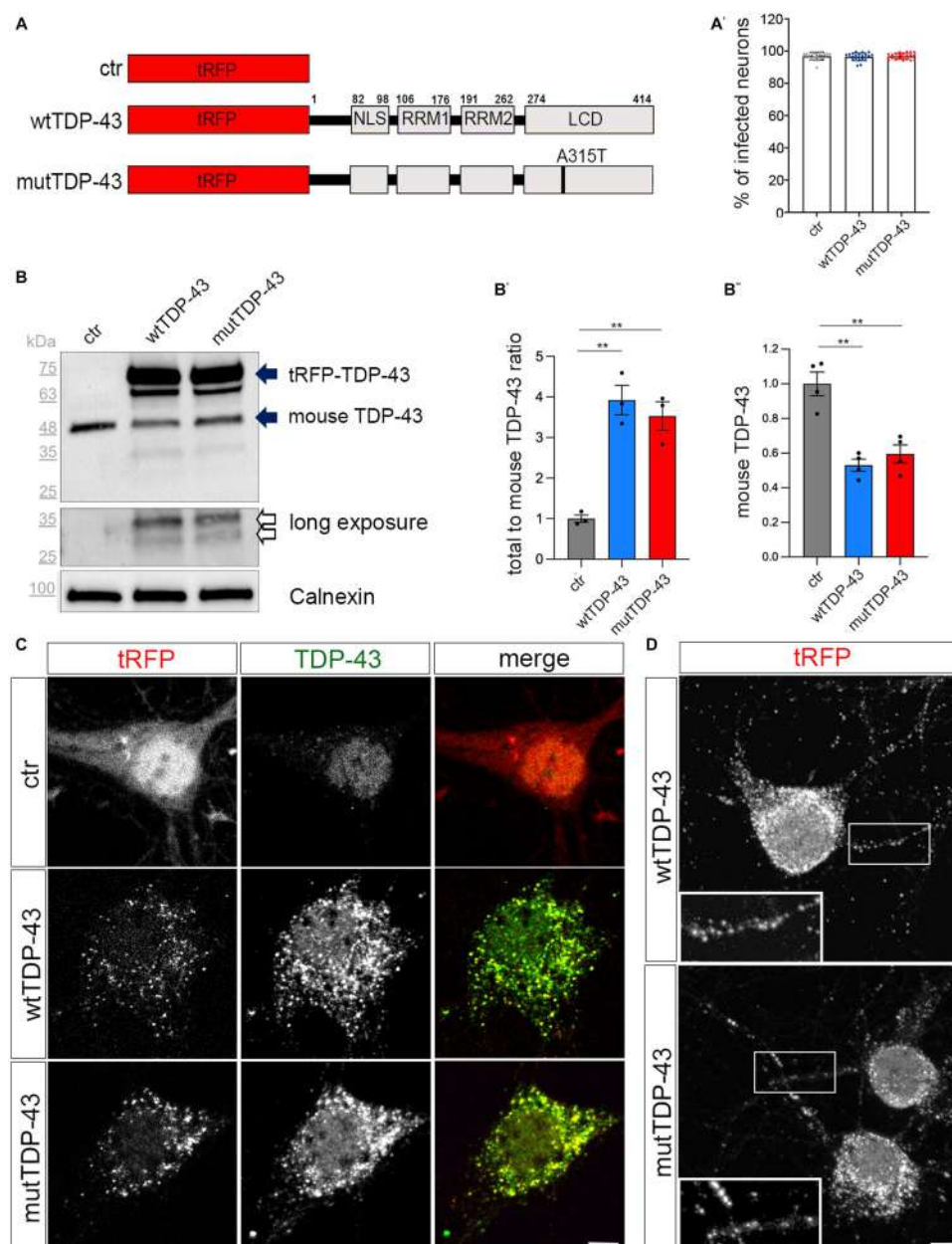


FIGURE 1

Cytoplasmic aggregate formation in neurons expressing tRFP-TDP-43. **(A)** Schematic representation of ctr, wtTDP-43 and mutTDP-43 constructs. TDP-43 functional domains are also shown. This schematic shows the presence of the fluorescent tag (tRFP) at the N-terminal position of TDP-43. NLS, Nuclear Localization Sequence; RRM1, RRM2, RNA Recognition Motif-1 and -2; LCD, low-complexity glycine-rich domain. The A315T aa substitution is located in the LCD domain. **(A')** Percentage of transduced neurons analyzed by the ArrayScan microscope on 3 independent experiments ($n=12,877$ for ctr, 9,381 wtTDP-43 and 11,634 mutTDP-43); each dot corresponds to the average percentage of a single microscope field. **(B)** Western blot of protein lysates derived from ctr, wtTDP-43 and mutTDP-43 neurons immunostained with an Ab detecting both human and murine TDP-43. An anti-calnexin Ab was used as a loading control. The ~75kDa band (upper solid arrow), corresponds to the product of tRFP N-terminally fused with human TDP-43 (wt or A315T); the ~48kDa band corresponds to endogenous murine TDP-43 (lower solid arrow). Another band (~63kDa) is present in TDP-43-overexpressing neurons, likely representing a C-terminal cleavage product of the fusion protein. Upon a longer exposure, two additional bands appear (empty arrows). **(B')** The graph shows the ratio of total TDP-43 levels (human + endogenous mouse protein) to endogenous TDP-43 levels in ctr cells. Panel **(B'')** shows the normalized level of endogenous TDP-43 in TDP-43-overexpressing neurons relative to ctr ones. Values are expressed as mean \pm SEM; **B'**: $n=3$; **B''**: $n=4$; Kruskal-Wallis test (non-parametric), $**p<0.01$. **(C)** Ctr, wtTDP-43 and mutTDP-43 neurons at 14 DIV, immunostained with an Ab detecting both human and murine TDP-43 (green). In ctr neurons, tRFP is concentrated mostly in the nucleus, while exogenous tRFP-TDP-43 (wt or A315T) is highly enriched in the cytoplasm of wtTDP-43 and mutTDP-43 neurons, forming aggregates. Size bar: 5 μ m. **(D)** wtTDP-43 and mutTDP-43 aggregates, revealed by tRFP fluorescence, are found not only in cell bodies but also in neurites (see magnification in insets). Size bar: 5 μ m.

(Neumann, 2009; Ling et al., 2013). TDP-43 is known to bind other RBPs (e.g., fragile X mental retardation protein, FMRP, and neuron-specific Elav-like Hu RNA-binding protein D, HuC/D), generating granules that transport mRNAs along neurites (Fallini et al., 2012).

Therefore, we investigated the nature of exogenous TDP-43 aggregates in our UMN cultures by immunostaining wtTDP-43 and mutTDP-43 neurons with an HuC/D-specific Ab. HuD is involved in mRNA stability, splicing, and positive regulation of translation (Diaz-Garcia

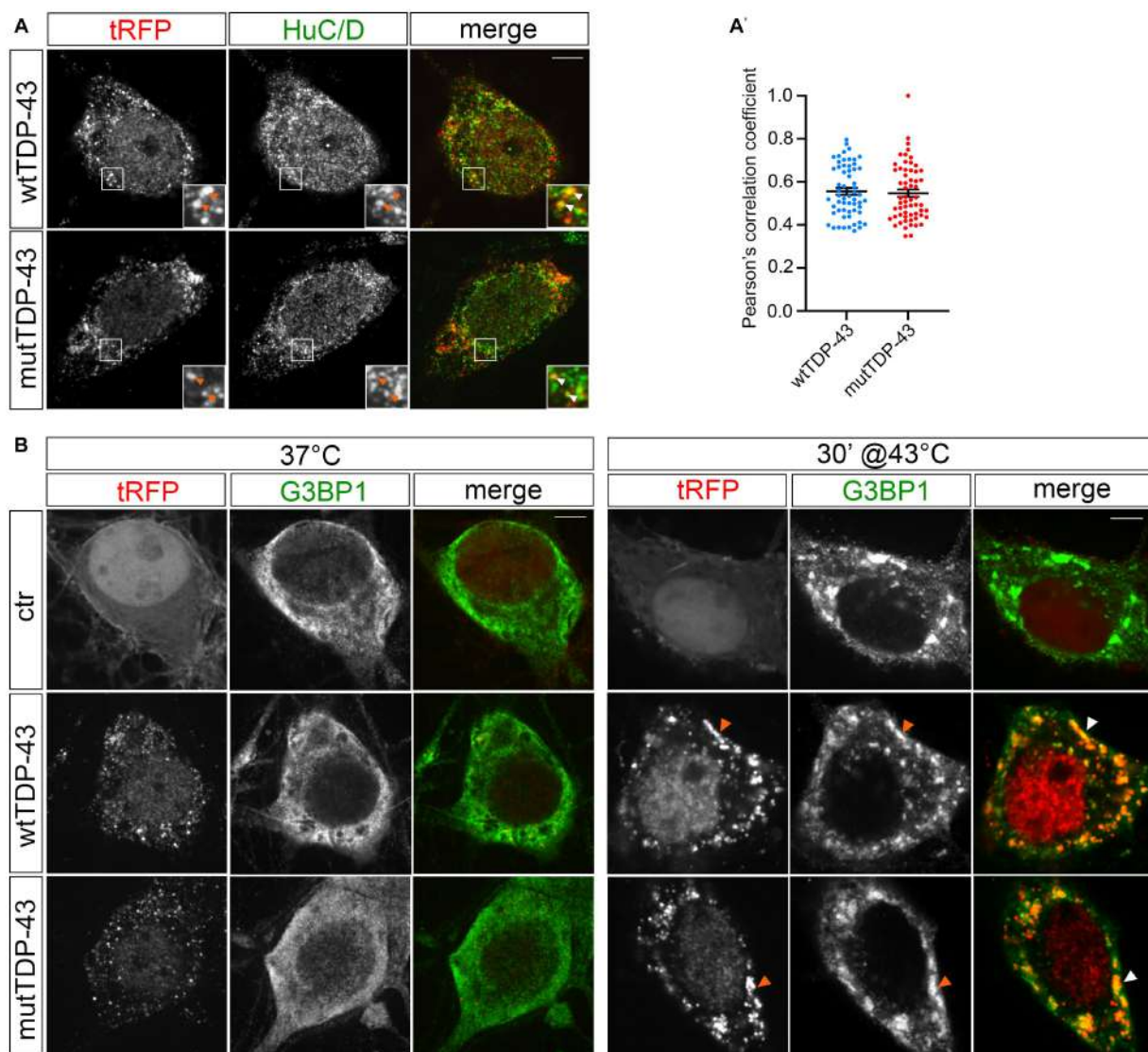


FIGURE 2
tRFP-TDP-43 is recruited by RNA granules. **(A)** Immunofluorescent staining of wtTDP-43 and mutTDP-43 neurons with an anti-HuC/D antibody. HuC/D (green) partially colocalizes with fluorescent tRFP-TDP-43 aggregates (wt or A315T; red) as shown by arrowheads in insets. **(A')** Dots in histogram indicate the percentage of HuC/D-tRFP colocalization in each individual cell examined; mean positive Pearson's correlation coefficient: $r = 0.56 \pm 0.016$ (wtTDP-43); 0.55 ± 0.017 (mutTDP-43; Mean \pm SEM, $n = 3$). **(B)** Immunofluorescence of ctr, wtTDP-43 and mutTDP-43 neurons with anti-G3BP1 under physiological conditions (left) and after heat shock (right).

et al., 2021). Our results reveal that exogenous TDP-43 granules partially colocalize with HuC/D (Figure 2A). The degree of colocalization, plotted in Figure 2A', shows that HuD colocalizes slightly more frequently with wtTDP-43 than with mutTDP-43.

To assess whether exogenous TDP-43-positive cytoplasmic granules colocalize with stress granules (reviewed in Dewey et al., 2012), we immunostained cells for Ras-GTPase-activating protein SH3 domain-binding protein 1 (G3BP1), a known component of stress granules that is involved in their formation (Matsuki et al., 2013). Under basal conditions (37°C), G3BP1 signal displayed a diffuse pattern in ctr, wtTDP-43 and mutTDP-43 neurons alike, while heat shock treatment (43°C, 30 min) generated G3BP1+ granules that contained exogenous TDP-43 (Figure 2B). This result recapitulates findings obtained in cells undergoing a

non-lethal injury (Higashi et al., 2013) and suggests that in our conditions TDP-43 does not promote SG formation *per se*, but retains the ability to be recruited to newly assembled stress granules, once they form (Colombrita et al., 2009), although TDP-43 oligomerization and aggregation takes place in the cytoplasm separate from them (Streit et al., 2022).

Global downregulation of protein synthesis in the axon of TDP-43-overexpressing mouse cortical neurons

In parallel to the functional analysis of our cellular models (see below), we took advantage of a transcriptome and translato-

(G. Viero and co-workers, Institute of Biophysics, CNR Unit at Trento; GEO ID: GSE239419) conducted on cell-body and axonal compartments, to explore the gene expression and mRNA translation landscape at a systems biology level. To this end, cortical neurons were plated on microfluidic chambers (Taylor et al., 2005), consisting of two main channels separated by 450 μm -long microgrooves (see Methods); cell bodies are too large to enter them, while dendrites are too short to extend beyond them.

The physical separation of axonal and somatodendritic compartments was demonstrated by immunofluorescence in untransduced neurons, cultured in microfluidic chambers for 9 DIV and immunostained with Abs for Microtubule Associated Protein 2 (MAP2), a dendrite-specific marker, and for TuJ1, which decorates dendrites, cell bodies and axons alike. As shown in [Supplementary Figure 4](#), MAP2 signal is sharply restricted to the whole-cell channel, while axons extend the right channel and are labeled by TuJ1 only.

To ask whether exogenous TDP-43 might bind to components of the mRNA translation machinery, possibly affecting local mRNA translation in the axon, we immunostained wtTDP-43- and mutTDP-43-expressing neurons with antibodies against small and large ribosomal subunit proteins (RPS6 and RPL26, respectively). As shown in [Figure 3A](#) and histogram in [Figure 3A'](#), 20% of granules, on average, colocalize with RPS6 and RPL26, in both wtTDP-43 and mutTDP-43 neurons. This finding suggests that TDP-43 aggregates may sequester ribosome components and/or interfere with ribosomal transport, likely resulting in an overall decrease of mRNA translation.

Therefore, we set out to determine whether wtTDP- and mutTDP-expressing neurons showed decreased axonal levels of RPL26, a component of the ribosomal large subunit for which efficient antibodies are available, relative to control axons. To this end, we immunostained wtTDP-43, mutTDP-43 and ctr neurons, cultured in microfluidic chambers for 9 DIV, with antibodies to RPL26 and the axonal marker TuJ1. RPL26 signal was then quantified in the axon and cell body. As shown in [Figures 3B,B'](#), RPL26 protein levels are decreased in both axons and cell bodies of wtTDP-43 and mutTDP-43 neurons relative to ctr neurons. In conclusion, the decrease of axonal RPL26 suggests that the overall amount of 60S ribosomal subunit may be significantly reduced in wtTDP-43 and mutTDP-43 axons and cell bodies, relative to ctr neurons.

Accordingly, we asked if protein synthesis might be globally defective in these neurons. To assess whether mRNA translation is affected in wtTDP-43 and mutTDP-43 neurons, we carried out a puromycylation assay (David et al., 2012). By quantitative immunofluorescence methods, we evaluated puromycin incorporation as a measure of ongoing protein synthesis. As shown in [Figures 3C,C'](#), in both wtTDP-43 and mutTDP-43 neurons puromycin signal is significantly reduced in the cell body, axon and growth cone alike, similar to findings previously observed at the neuromuscular junction (Altman et al., 2021).

To identify transcripts downregulated in the axon of wtTDP-43 and mut-TDP-43 neurons, next-generation sequencing (NGS) of the axon- and cell-body-specific polysome-engaged mRNAs (polysome profiling) from TDP-43-overexpressing neurons was performed by tag-free polysome isolation through a miniaturized sucrose gradient ([Supplementary Figure 5](#); see Methods, Negro et al., 2018).

We found that polysomal mRNA levels are robustly dysregulated in both human TDP-43-expressing neuronal populations compared to control neurons, with 1,598 and 1,601 differentially expressed genes (DEGs) for wtTDP-43 and mutTDP-43, respectively. Compared to the number of DEGs in the cell body alone (467 in human TDP43 and 513 in mouse TDP43), more changes occur in the axon, accounting for 65 and 68% of total DEGs, respectively. Importantly, 1,043/1,131 (92%) axonal DEGs in wtTDP-43 and 877/1,088 (81%) in mutTDP-43 are downregulated, suggesting a widespread loss of mRNAs engaged in local translation ([Table 1](#)).

Of all downregulated polysome-engaged transcripts, a large number belonged to gene ontologies related to protein synthesis and displayed lower levels in wtTDP-43 and mutTDP-43 neurons (289 and 313, respectively), compared to control neurons ([Figure 3D](#)). Of these, 47 axon-specific polysome-engaged DEGs were shared between the two overexpressing populations, and are listed in [Table 2](#) and [Supplementary Table 1](#). Remarkably, in wtTDP-43 neurons, axon-specific polysomal DEGs make up 97.6% of the total, whereas in mutTDP-43 cells axon-specific DEGs amount to 33.9% of the total.

Increased oxidative stress in TDP-43-overexpressing neurons

Two other gene ontologies affected by TDP-43 overexpression were related to synaptic function and to the response to oxidative stress. The presence of high levels of ROS and the consequent oxidative stress-dependent neuronal damage are among the main hallmarks of ALS (Barber and Shaw, 2010). Therefore, we asked whether our neuronal model of TDP-43 proteinopathy exhibits this characteristic aspect of neurotoxicity. We performed this analysis in neurons loaded with H_2DCFDA (DCF), both under untreated conditions ([Figure 4A](#)) and upon mild iron overload (48 h in the presence of 20 μM ferric iron); the latter provides information about the ability of neurons to counteract and detoxify an oxidative condition, promoted here by the iron-catalyzed Fenton reaction. Not only did our results show a significant increase in basal ROS levels in both overexpressing populations compared to ctr neurons ([Figure 4B](#), red dot bars), but they also revealed a sharply increased oxidative effect of iron overload in TDP-43 overexpressing neurons vs. ctr cells ([Figure 4B](#), green dot bars). As mentioned, numerous polysome-engaged somatic and axonal mRNAs involved in the response to oxidative stress are downregulated in neurons expressing wtTDP-43 (78) and mutTDP-43 (74), compared to ctr neurons. Notably, a majority of differences observed in wtTDP-43 neurons were relative to axonal mRNAs, suggesting that locally translated axonal mRNAs may play a major and as yet uncharacterized role in the detoxification of oxidative stress. Out of the axonal DEGs, 9 were shared between wtTDP-43 and mutTDP-43 neurons ([Figure 4C](#); [Table 2](#); [Supplementary Table 1](#)), and include transcripts encoding nucleotide exchange factors for chaperone proteins, kinases, ER membrane sensors involved in stress response and *Prdx2*, encoding an abundant cytosolic peroxidase.

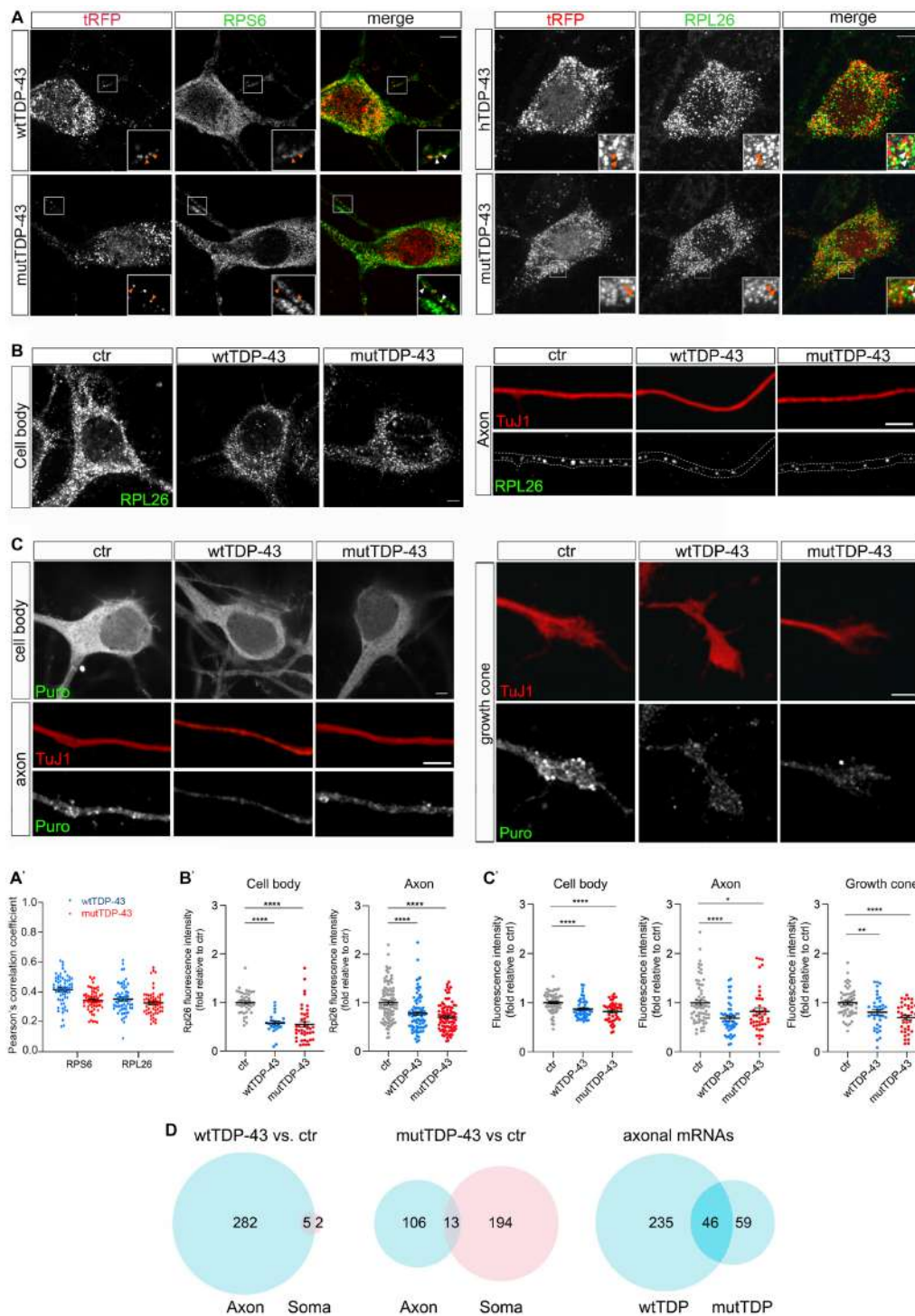


FIGURE 3

Axonal protein synthesis is reduced in wtTDP-43 and mutTDP-43 neurons. **(A)** A fraction of small and large subunit ribosomal proteins (RPS6 and RPL26, respectively) colocalize with aggregates of RFP-tagged human TDP-43, both wild type and mutant (see arrowheads in insets). **(A')** Dots in histograms indicate the percentage of colocalization in each individual cell examined; mean positive Pearson's correlation coefficient: for RPS6, $r = 0.41 \pm 0.013$ (wtTDP-43); 0.34 ± 0.009 (mutTDP-43); for RPL26, $r = 0.35 \pm 0.013$ (wtTDP-43); 0.33 ± 0.012 (mutTDP-43); (Mean \pm SEM, $n = 3$). **(B)** RPL26 protein abundance is reduced in the cell body (left) and axon (right) of cells expressing human TDP-43, wt or mutant. Differences and their statistical significance are plotted in **B'**, where each dot corresponds to an individual cell or axon examined. Mean \pm SEM, $n = 3$, Mann-Whitney test (non-parametric), ****value of $p < 0.0001$. **(C)** Global protein synthesis, expressed as the intensity of puromycin-positive signal, is decreased in the cell body, axon and growth cone of cells expressing human TDP-43, wt or mutant (see results for explanation). Differences and their statistical significance are plotted in **C'**, where each dot corresponds to an individual cell/axon/growth cone (Mean \pm SEM, $n = 3$, Mann-Whitney test (non-parametric), *value of $p < 0.05$, **value of $p < 0.01$, ****value of $p < 0.0001$). **(D)** Here and in subsequent figures, the Venn diagrams on the left and in the center show the number of DEGs in the axon (light blue) and soma (pink) of wtTDP-43 and mutTDP-43 neurons, respectively; the intersection between blue diagrams on the right indicates axonal DEGs shared by the two populations, and listed in Table 2. Venn diagrams shown here describe the numbers of polysome-engaged mRNAs, involved in various aspects of mRNA translation, whose abundance is decreased in wtTDP-43 and mutTDP-43 axons vs. ctr ones. Note the high number of axonal DEGs belonging to gene ontologies related to mRNA translation.

TABLE 1 Upregulated and downregulated DEGs in human TDP-43 expressing neurons vs. controls.

		Cell body	Axon
wtTDP-43	Upregulated	86	88
	Downregulated	381	1,043
	Total	467	1,131
mutTDP-43	Upregulated	85	211
	Downregulated	428	877
	Total	513	1,088

TABLE 2 Downregulated axonal mRNAs shared by wtTDP-43 and mutTDP-43 neurons.

Gene ontology category	Genes
mRNA translation/protein synthesis	Celf1, Cnot7, Eef1b2, Eif4g1, Eif4g2, Eif4g3, Eif5a, Fus, Fxr1, Gapdh, Gm6576, Gm8210, Hspa8, Ilf3, Myc, Nop56, Npm1, Pabpc1, Pcbp2, Ptbp1, Pum2, Rbm4, Rbm4b, Rock2, Rpl11, Rpl14, Rpl22, Rpl3, Rpl30, Rpl35a, Rpl5, Rpl6, Rpl7, Rpl9, Rplp2, Rps12, Rps13, Rps15a, Rps2-ps6, Rps24, Rps7, Rps8, Rps9, Snu13, Srp54b, Xpo1, Zfp706
Oxidative stress	Becn1, Clcn3, Hsph1, Map3k7, Mapk9, Nfe2l1, Prdx2, Rock2
Synaptic function	Abi1, Abi2, Abr, Actr3, Adgrl1, Adgrl3, Afdn, Agrn, Agtppb1, Akap7, Ap1ar, Apbb1, Arhgap21, Arhgef9, Atp2b2, Bsg, Cadm1, Camk2d, Cask, Clcn3, Clta, Copa, Copg2, Cux1, Dclk1, Dlg4, Dlgap1, Dst, Epb41l2, Erbin, Flna, Fus, Fxr1, Gapdh, Gapvd1, Gdi1, Gls, Gnas, Gpm6b, Hnrnpa2b1, Hspa8, Kif3c, Macf1, Malat1, Map2, Map3k7, Mapk9, Mia2, Ncoa2, Ndrgr4, Nfia, Nrnx2, Pak3, Pebp1, Plekha5, Psma3, Ptk2, Rapgef1, Rims1, Rnf10, Rock2, Scn1a, Scn8a, Sgip1, Sh3kbp1, Stxbp1, Syne1, Synj1, Syt7, Tln2, Tmcc1, Tmod2, Tnik, Ube2i, Usp48, Ywhaq, Zfp365

Impaired spontaneous electrical activity, calcium handling and synaptic function in TDP-43 overexpressing neurons

As mentioned, gene ontologies related to synaptic function are affected in wtTDP-43 and mutTDP-43 neurons, compared to ctr neurons. Synaptic abnormalities have been reported in the neurons of both ALS patients and animal models (primarily *SOD1* transgenics), ranging from morphological alterations to functional impairment, thereby supporting the hypothesis that ALS might either result from, or be exacerbated by synaptic dysfunction (Fogarty, 2019).

Since synaptic alterations seem to involve primarily glutamatergic neurons, as suggested by recent genetic studies (van Rheenen et al., 2021), we investigated whether wtTDP-43 and mutTDP-43 overexpression could induce synaptic impairment in our cultures. Whole-cell patch clamp experiments revealed spontaneous, AMPA-dependent mini excitatory postsynaptic currents (mEPSCs), recorded at a holding potential of -70 mV and in the presence of a Na^+ channel blocker (TTX, $1 \mu\text{M}$) and GABA_A receptor antagonist (gabazine, $10 \mu\text{M}$). No significant differences were detected in the average amplitude, decay time constant, or frequency of mEPSCs (Supplementary Figure 6). However, spontaneous synaptic activity in TTX- and gabazine-free ACSF revealed recurrent bursts of postsynaptic currents (Figure 5A). While burst duration was not affected by TDP-43 overexpression (Figure 5A''); either wild-type or mutant), the frequency of bursts was significantly reduced in both overexpressing populations compared to ctr neurons (Figure 5A').

The decrease of spontaneous bursting activity observed in TDP-43 overexpressing neurons prompted us to investigate the role of calcium (Ca^{2+}) homeostasis in UMNs. To this end, neurons were loaded with the fura-2 calcium dye which, thanks to its ratiometric properties, makes it possible to compare intracellular Ca^{2+} levels both at rest and at maximal glutamate ($100 \mu\text{M}$) stimulation. In keeping with the

decreased burst frequency, both wtTDP-43 and mutTDP-43 UMNs showed decreased basal levels of intracellular Ca^{2+} concentration [Ca^{2+}]_i compared to ctr neurons, therefore potentially affecting spontaneous electrical activity. Notably, the amplitude of [Ca^{2+}]_i response to glutamate stimulation was also significantly reduced in wtTDP-43 but not in mutTDP-43 neurons (Figure 5B).

The impairment of spontaneous synaptic activity correlates with a depletion of vesicles in presynaptic active zones in TDP-43-overexpressing neurons, as revealed by ultrastructural analysis (Figure 5C) and by the quantification of presynaptic vesicle numbers (graph in Figure 5C'). To confirm in live neurons the results obtained by electron microscopy, we exploited the properties of the FM1-43 dye (Amaral et al., 2011), since the loading and loss of the fluorescent dye provide a reliable measurement of synaptic vesicle retrieval and release in cultured neurons (Sambri et al., 2020). Exo-endocytosis was evoked by a first pulse of depolarizing stimulus (30 mM KCl added to the bath together with FM1-43 dye; see Methods); after washing the non-vesicle bound FM1-43, we quantified the fluorescence signal within synaptic boutons, correlating with their content of endocytic FM1-43-labeled vesicles (see image in Figure 5D, left image). The graph in Figure 5D' shows a trend of signal decrease in wtTDP-43 neurons and a sharp decrease in mutTDP-43 cells, indicating, as in graph Figure 5C', a lower number of vesicles in TDP-43-overexpressing neurons compared to ctr ones. The FM1-43-based experiments also allowed us to analyze the rate of synaptic exocytosis; indeed, after inducing fluorescent dye endocytosis, a second depolarizing KCl pulse caused vesicle exocytosis, evaluated by FM1-43 fluorescence decay over 20 s. As shown in Figure 5D (right) and Figure 5D'' mutTDP-43 and, even more so, wtTDP-43 neurons, where calcium alterations are more pronounced, show a major impairment in their rate of exocytosis compared to ctr cells.

Again, a high number of DEGs were observed in the axonal translome, underlying the key contribution of axonal protein

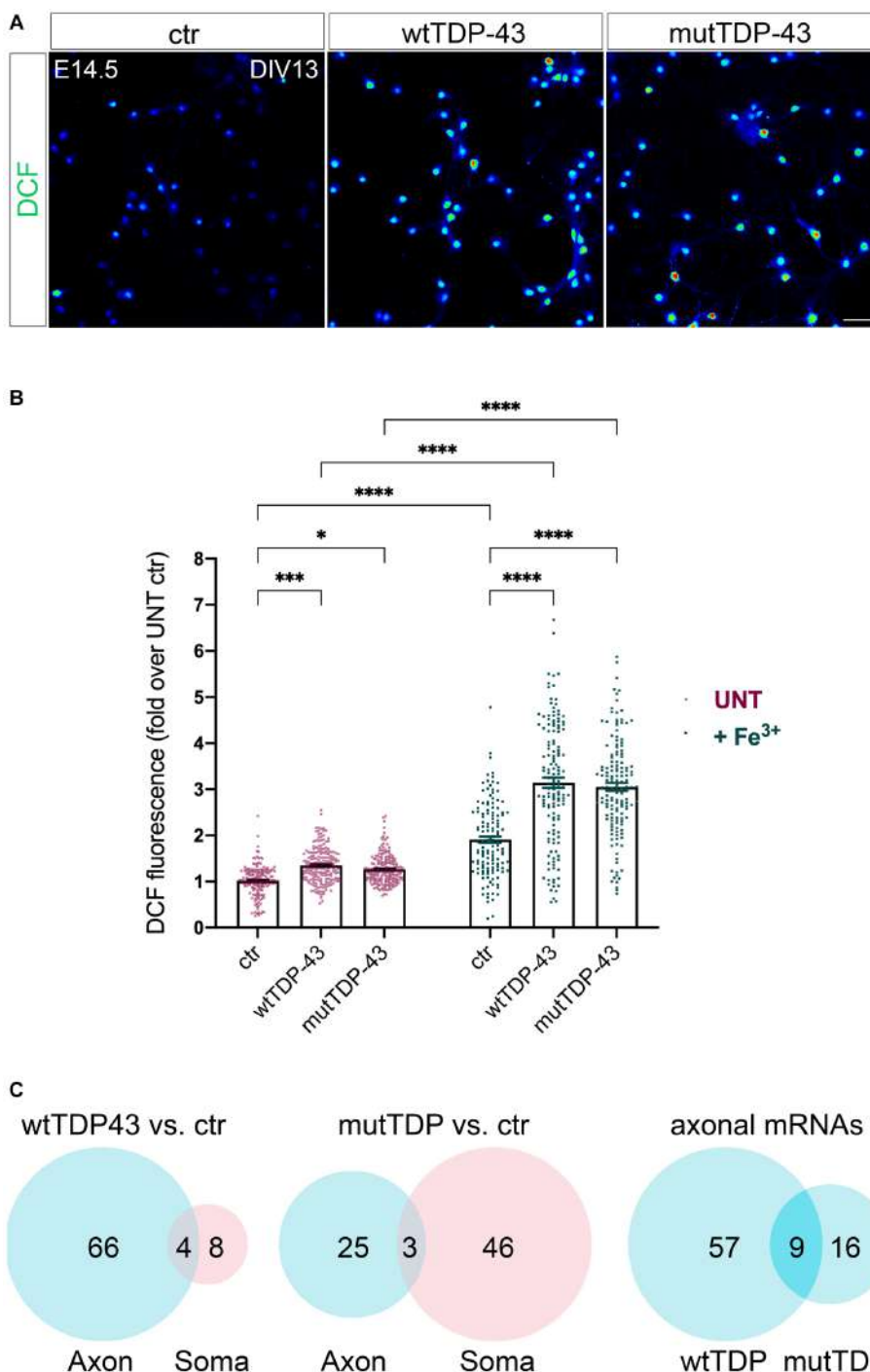


FIGURE 4 Impairment of the response to oxidative stress in neurons wtTDP-43 and mutTDP-43 neurons. **(A)** Representative images of ctr, wtTDP-43 and mutTDP-43 neurons loaded with DCF (green) shown as rainbow look-up table (LUT) values. **(B)** Graph showing DCF fluorescence intensity of ctr, wtTDP-43 and mutTDP-43 relative to untreated (UNT) ctr neurons, in the absence (red) or presence (green) of Fe³⁺ treatment. Data are expressed as mean ± SEM, from 4 or 5 biological replicates; each dot corresponds to an individual microscope field (n = 48 fields for each experimental condition with an average of 60–70 neurons/field); Two-way ANOVA test *p < 0.05; ***p < 0.005; ****p < 0.0001. **(C)** Venn diagrams reporting the numbers of downregulated polysomal DEGs involved in the response to oxidative stress. Note the high number of mRNAs, belonging to gene ontologies related to oxidative stress, which show differential abundance in the axon.

synthesis to the regulation of synaptic activity and maintenance (Figure 5E). The list of significantly downregulated synaptic mRNAs shared by wtTDP-43- and mutTDP-43 axons includes transcripts

encoding synaptic adhesion molecules, regulators of cytoskeletal dynamics, regulatory and structural proteins involved in synaptic vesicle trafficking/recycling (Table 2; Supplementary Table 1).

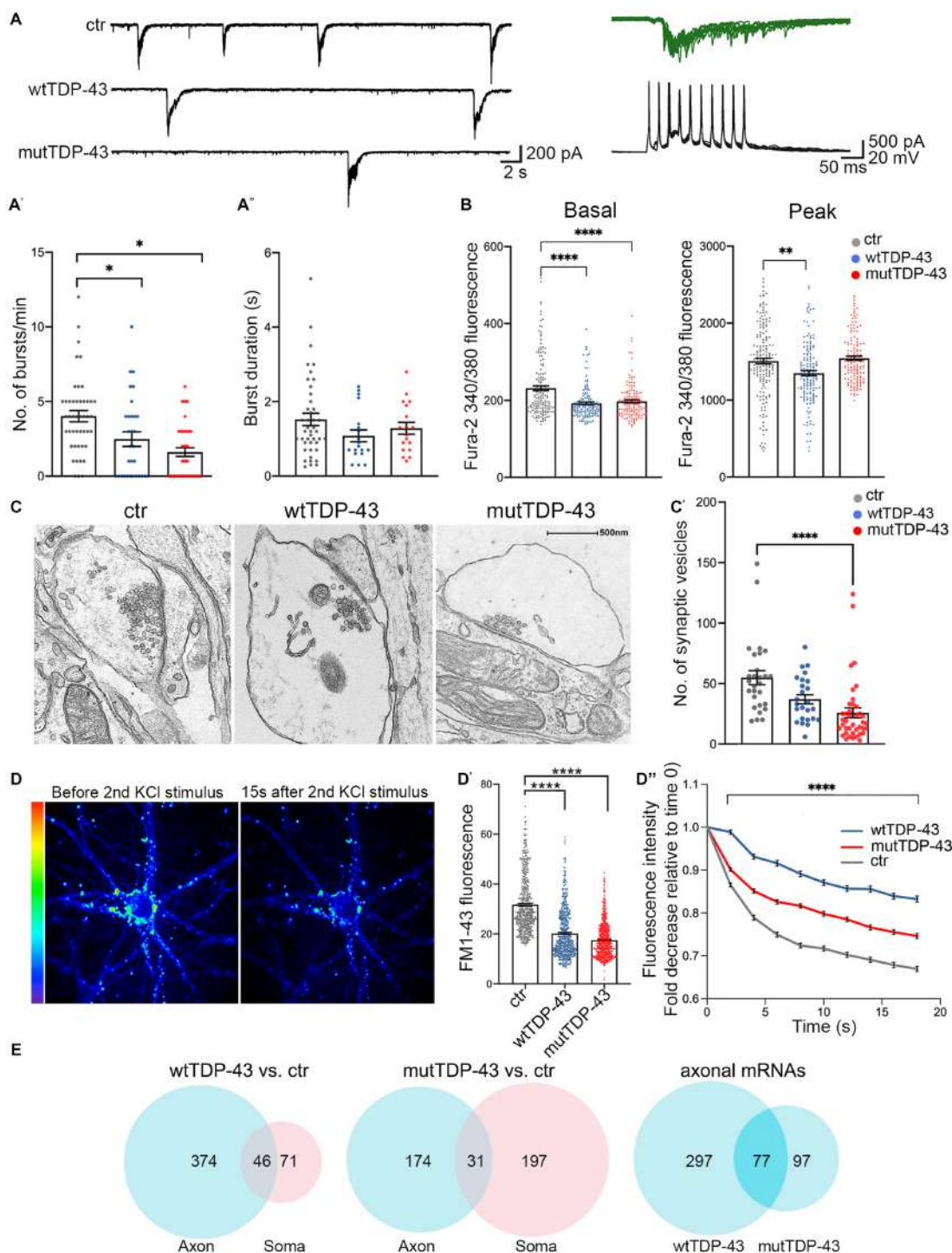


FIGURE 5

Impairment of spontaneous burst firing, calcium responses and synaptic vesicle exocytosis in neurons expressing human TDP-43. (A) Top left: examples of spontaneous compound postsynaptic current (PSC) bursts recorded in ctr, wtTDP-43, and mutTDP-43 cultures. Top right: individual PSC bursts recorded in voltage clamp mode at a V_h of -70 mV correlate with spontaneous action potential bursts recorded in current clamp in a different cell. (A') Summary plots of average burst frequencies. (A'') Average duration of individual bursts. wtTDP-43 and mutTDP-43 show decreased burst frequency relative to ctr, while no difference in individual burst duration was observed (Mean \pm SEM, of 46 ctr neurons, 31 wtTDP-43 neurons and 41 mutTDP-43 neurons, from 12, 11, and 10 experiments, respectively), Mann Whitney U -Test (non-parametric), $ns = p > 0.05$, $*p < 0.05$. (B) Graphs showing fura-2 340/380 nm ratio of fluorescence intensity in ctr, wtTDP-43 and mutTDP-43 neurons under basal conditions (graph on the left) and at the peak of response after glutamate stimulation [graph on the right; Mean \pm SEM of 176 ctr neurons, 158 wtTDP-43 neurons, and 151 mutTDP-43 neurons, from 5 biological replicates, Kruskal-Wallis test (non-parametric), $**p < 0.001$, $****p < 0.0001$]. (C) Transmission electron microscopy analysis reveals synaptic boutons and the corresponding postsynaptic side. Note a significant reduction of vesicle numbers in mutTDP-43 neurons. (C') Synaptic vesicle counts were performed on electron microscopy images from 4 different biological replicates using ImageJ software. In particular we counted 28 images for trFP ($n = 1,536$ synaptic vesicles), 26 for wtTDP-43 ($n = 1,099$ synaptic vesicles); 40 for mutTDP-43 ($n = 1,032$ synaptic vesicles); Mean \pm SEM, Kruskal-Wallis

(Continued)

Figure 5 (Continued)

test (non-parametric), **** $p < 0.0001$. **(D)** Representative images showing FM1-43 fluorescence intensity as rainbow LUTs at two time points of the FM1-43 assay. The left image shows a neuron after treatment with 10 μ M FM1-43 and 30mM KCl simultaneously to promote internalization of the dye in synaptic vesicles; the right image shows FM1-43 fluorescence intensity 15s after the second stimulus with 30mM KCl, which triggers exocytosis of fluorescence-loaded vesicles. **(D')** The graph shows fluorescence levels of synaptic contacts upon completion of endocytosis (e.g., left panel in **D**), revealing a significant decrease of FM1-43 signal in both wtTDP-43 and mutTDP-43 cells; Mean \pm SEM, Kruskal-Wallis test (non-parametric, **** $p < 0.0001$). This result parallels the number of vesicles loaded with FM1-43. **(D'')** Graph showing the decay of FM1-43 fluorescence relative to time 0, upon addition of the 2nd KCl stimulus, in wtTDP-43 (blue), mutTDP-43 (red) and ctr cells (gray). The downward slope of the curve parallels the rate of exocytosis [Mean \pm SEM, from 5 biological replicates, Mann-Whitney test (non-parametric), ****value of $p < 0.0001$, number of analyzed ROI: ctrl=456, wtTDP=384, mutTDP=532]. **(E)** Venn diagrams reporting the numbers of downregulated polysomal DEGs involved in synaptic function. Note the high number of differentially abundant mRNAs, belonging to gene ontologies related to synapses, which show differential abundance in the axon.

Discussion

In this study, we report the generation and functional characterization of mouse UMN, transduced with wt and mutant forms of TDP-43 for use as neuronal models of TDP-43 proteinopathy. Primary cortical neuron cultures often contain a heterogeneous neuroglial population, which makes it difficult to discriminate neuronal cell-autonomous mechanisms from the effects of glial-neuron interactions. However, the neuronal cultures described here are highly homogeneous and almost entirely comprised of TBR1-positive glutamatergic projection neurons of the deep cortical layers, the cerebral neuron type that is most sensitive to ALS (Limone et al., 2021), in the virtual absence of GABAergic neurons or glial cells.

TDP-43 proteinopathy, which manifests itself as nuclear depletion and cytoplasmic accumulation/aggregation of TDP-43, is a very frequently observed feature of ALS (Arai et al., 2006; Neumann et al., 2006; de Boer et al., 2020). While animal models displaying physiological levels of TDP-43 aim at faithfully reproducing the pathophysiology of the disease, they often show a mild phenotype that can be properly analyzed only at late stages. The Q331K TDP-43 knock-in mouse model (White et al., 2018) shows almost no motor dysfunction nor TDP-43 proteinopathy, although it exhibits a late cognitive phenotype. Likewise, a knock-in model, carrying the M323K mutation, exhibits a mild muscular phenotype with reduced grip strength only at 2 years of age and no TDP-43 pathology in the spinal cord or brain; however, at the molecular level, these mice show alterations in RNA splicing (Fratta et al., 2018). Conversely, our primary cultures of UMN exhibit spontaneous cytoplasmic TDP-43 aggregate formation.

Although the use of fluorescently tagged TDP-43 has been reported to impair its nuclear egress (Ederle et al., 2018), this is not the case in our models. Instead, we hypothesize that the size of the RFP-TDP-43 fusion protein may hinder its nuclear import, causing trafficking defects akin to those produced by NLS removal (Igaz et al., 2011). This facilitates the formation of cytoplasmic TDP-43 aggregates, which are not observed upon overexpression of RFP alone. This feature is reminiscent of the pathological aggregates observed in the cerebral cortex and spinal cord of familial and sporadic ALS patients (Mackenzie et al., 2011; Diaz-Garcia et al., 2021), effectively mimicking TDP-43 proteinopathy. Taken together, these features make our primary cultures a useful tool for the study of TDP-43 proteinopathy, within the ephemeral lifespan of a primary culture. Our models provide a solid screening platform suited to produce new evidence amenable to validation in other, more physiological model systems.

While the cytoplasmic aggregates described here are positive for established RNA granule markers (Sidibé and Vande Velde, 2019), defining the complete nucleotide and peptide composition of those

aggregates will require further studies. In fact, mRNA granules recruit multiple factors. Importantly, TDP-43+ granules recruit other RNA-binding proteins, such as FMRP, IMP and HuD (Fallini et al., 2012), possibly sequestering an additional mRNA population via protein-protein interactions. Notably, tRFP-TDP-43 fusion proteins form aggregates in the absence of overt cellular stress, indicating that tRFP-TDP-43 overexpression does not *per se* induce acute cellular stress.

Our results suggest that RFP-TDP-43+ granules sequester proteins required for mRNA translation, likely reducing the global rate of protein synthesis in the cell body, dendrites and axon alike. In keeping with this observation, RPL26 protein levels are profoundly reduced in the axon of wtTDP-43 and mutTDP-43 neurons. Moreover, the results of our puromycylation assay directly show an overall decrease in axonal protein synthesis; in fact, the levels of numerous polysome-engaged mRNAs involved in protein synthesis are significantly decreased in the axon of TDP-43 overexpressing neurons. Such mRNAs are deregulated in the axon of both overexpressing populations, and encode, among others, translation initiation factors and RNA-binding proteins. One open question regards the role of transcripts encoding ribosomal proteins in the axon (Nagano et al., 2020); recent evidence suggests that they may subserve the repair of damaged ribosomes (Fusco et al., 2021).

Our functional analysis also revealed that wtTDP-43 and mutTDP-43 neurons exhibit increased oxidative stress levels, a hallmark of ALS neurons (reviewed in Barber and Shaw, 2010), and they do so in the absence of glial cells, suggesting that a neuronal-autonomous/paracrine mechanism may contribute to the alteration of redox homeostasis in neurons displaying TDP-43 proteinopathy. Importantly, wtTDP-43 and mutTDP-43 neurons show a basal increase of ROS production, indicating a chronic oxidative condition; moreover, these neurons display a reduced ability to counteract a condition of iron overload, used here to mimic the signs of iron accumulation that have been detected in the motor cortex (Bhattarai et al., 2020), frontal operculum, and precentral gyrus (Mitani et al., 2021) of ALS patients. Iron overload may, in turn, affect not only the neuronal reducing potential, but also calcium homeostasis and synaptic function (Pelizzoni et al., 2008). We found that several mRNAs relative to the oxidative stress response are underrepresented in the axon of wtTDP-43 and mutTDP-43 neurons; thus, it is reasonable to hypothesize that axonal translation may contribute importantly to the control of oxidative stress and that, in tract neurons projecting very long axons, this contribution may be extremely important; in fact axons account for >95% of the total neuronal volume.

Among the downregulated axonal mRNAs, *Prdx2* is highly expressed in normal spinal motoneurons (Kato et al., 2004) and plays an essential role in detoxifying hydrogen peroxide. Peroxiredoxins protect neurons from oxidative stress (Bettegazzi et al., 2019) and their

reduced level in ALS neuronal axons might therefore contribute to functional alterations of UMNs (Liu et al., 2020). *Prdx2* is temporarily upregulated in the spinal cord of presymptomatic SOD1 mice (Pharaoh et al., 2019) and in surviving ALS patients' motoneurons at an intermediate disease stage, while at late stages the breakdown of this antioxidant system accelerates neuronal death (Kato et al., 2005). Further studies are required to assess whether *Prdx2* plays a protective role in ALS/FTD neuronal models.

With respect to synaptic activity, repeated bursts of postsynaptic currents, which represent a typical electrical activity pattern scored in mature cortical neuron cultures, were sharply and significantly decreased in our human TDP-43-expressing populations, while burst duration only showed a nonsignificant decreasing trend.

Burst activity is often mediated by an increase of intracellular calcium (Helmchen et al., 1999; Larkum et al., 1999; Williams and Stuart, 1999), and the decrease in burst frequency observed in wtTDP-43 and mutTDP-43 neurons is in keeping with the finding that $[Ca^{2+}]_i$ is significantly reduced. Although several studies (*inter alia*, Perkins et al., 2021) found an opposite condition in ALS models, a reduction of hyperexcitability to a condition of hypoexcitability has been observed in human iPSC-derived neurons during their aging in culture (Sareen et al., 2013; Devlin et al., 2015; Naujock et al., 2016; Guo et al., 2017; Naumann et al., 2018; Sommer et al., 2022). The homogeneous composition of the culture system reported here reveals features that are intrinsic to glutamatergic neurons, unaffected by the contribution of astrocytes. Moreover, this result is also in agreement with the deregulation of calcium ion homeostasis observed in different ALS models and proposed as a pathophysiological hallmark of the disease; indeed, in addition to an alteration of glutamate neurotransmission, several mechanisms involved in calcium handling (e.g., plasma membrane calcium extrusion, calcium influx through AMPA glutamate receptors, and calcium import from endoplasmic reticulum into mitochondria) have been found altered in ALS motor neurons (Guatteo et al., 2007; Sirabella et al., 2018). Importantly, an impairment of presynaptic vesicle dynamics has been described in human iPSC-derived cortical neurons and spinal motoneurons from ALS patients (Jensen et al., 2020; Perkins et al., 2021; Aly et al., 2023). The significant decrease in exocytosis, revealed by FM1-43, is in agreement with the observation of reduced excitability, and may partially explain the disruption of connectivity observed in patients and animal models. Furthermore, the depletion of synaptic vesicles, revealed by EM, contributes to the global impairment of synaptic functions of human TDP-43-expressing neurons. Taken together, the decrease in PSC burst frequency in wtTDP-43 and mutTDP-43 cells was in accordance with reduced calcium responses and decreased vesicle availability at presynaptic terminals (which altogether may lower the probability of burst occurrence and synchronization across the synaptic network). The surprising observation that mEPSCs were unaffected may suggest that the probability of spontaneous, action potential-independent release of individual vesicles is less sensitive to the above mentioned changes, which likely influence massive events driven by strong presynaptic activation.

Our systems biology analysis shows that the levels of numerous polysome-engaged mRNAs encoding synaptic proteins is reduced both in the axon and cell body of human TDP-43-expressing neurons. Of note, a considerable number of downregulated transcripts involved in synaptic vesicle exocytosis (such as *Rab3a*, *Stx5a*, *Stx16*, *Snap25*, *Munc13*, *Rims1*, and *Syt7*), are selectively downregulated in

the axonal compartment of wtTDP-43 neurons, in keeping with the observation that exocytosis is more severely impaired in neurons transduced with wt TDP-43. Indeed, the expression of mutant TDP-43 may cause a more global impairment, affecting neuronal maturation, supported by the significantly decreased number of synaptic vesicles scored in this population (Figure 5C'). More broadly, the results of our translome analysis indicate that wtTDP-43 expressing neurons display a selective impairment of axonal mRNA translation, whereas cells expressing mutTDP-43 exhibit changes that affect the cell body and axon alike. As pointed out in the introduction, cytoplasmic accumulation of wtTDP-43 and subsequent aggregate formation is a feature of nearly all cases of ALS, most of which do not stem from *TARDBP* mutation. Our results support the notion that wtTDP-43 deregulation is a causal factor, not just a bystander effect in ALS pathology.

Polysomal mRNAs deregulated in the axon of wtTDP-43 and mutTDP-43 neurons control various aspects of presynaptic function, including cell adhesion, synapse formation, calcium responses, vesicular lumen acidification, glutamate synthesis, and neurotransmitter release. Likewise, a possible impairment of endocytosis is suggested by the reduced levels of transcripts involved in this phase of vesicle trafficking (Cremona et al., 1999; Mani et al., 2007; Miller et al., 2015).

The findings described here leave a key question unanswered, namely whether translation downregulation is restricted to TDP-43-bound mRNAs, possibly increasing the overall translation capacity for TDP-43-unbound transcripts.

Conclusion

This paper presents the results of multiple functional analyses performed on two cellular models of TDP-43 proteinopathy, the commonest neuropathological hallmark of ALS. The changes observed in our study correlate with a deregulation of axonal translation, further supporting its importance in the context of numerous homeostatic and functional processes. In particular, the prompt availability of proteins that are localized to the axon via slow axonal transport (Roy, 2020) may be critically dependent on local mRNA translation. This, among other factors, may account for the high sensitivity of long-range projection neurons to ALS.

Methods

Primary culture of cortical neurons

Animal handling and experimental procedures were performed in accordance with the EC guidelines (EC Council Directive 86/609/1987) and with the Italian legislation on animal experimentation (Decreto L.vo 116/92) and approved by our Institutional Animal Care and Use Committee.

Mouse embryonic cerebral cortices (strain C57BL/6N) were harvested at gestational day 14.5 (E14.5) and digested with Trypsin (Gibco, 15090-046). To obtain a single cell suspension the cells were mechanically dissociated with a glass Pasteur in neuronal culture medium (Neurobasal™ Plus Medium, Gibco A3582901, 1X B-27™ Plus Supplement, Gibco, A35828-01); the cell concentration was calculated with the T20 automated Cell Counter (Biorad). Cortical

neurons were plated at the density of 42,000/cm² on plastic or glass slides treated with Poly-D-Lysine (100 μg/mL, Sigma, P6407), and cultured in an incubator at 37°C, 5% CO₂. For specific experiments, cortical neurons were plated on microfluidic chambers (Xona Microfluidics, SND-450). In the cell body compartment, more neuron culture medium volume was added relative to the axonal compartment to generate hydrostatic pressure. At 2 days *in vitro* (DIV) 20 ng/mL BDNF (Proteintech, 450-02-B) was added to the axonal compartment; fresh BDNF (20 ng/mL) was added every 3 days.

Generation of lentiviruses expressing TDP-43 (wt and A315T)

For overexpression experiments in cortical neurons, we generated constructs encoding the human wt TDP-43 (wtTDP-43) and the human mutant TDP-43 (mutTDP-43), fused N-terminally with the turbo-Red Fluorescent Protein or the FLAG tag (DYKDDDDK, [Einhauer and Jungbauer, 2001](#)); the turbo-Red Fluorescent Protein (tRFP) was used as a control. For calcium assays control neurons were transduced with empty vector p277 instead of tRFP due to technical issues with the imaging instrument. The vectors were engineered in the laboratory, starting from the lentiviral vector pLenti277-GFP kindly provided by L. Naldini (San Raffaele-Telethon Institute of Gene Therapy, Milan, Italy). Lentiviral particles were prepared as described previously ([Amendola et al., 2005](#)). Briefly HEK293T cells were transiently co-transfected using the calcium-phosphate precipitation method with the transfer vectors, the MDLg/pRRE plasmid, the RSV-Rev plasmid and the MDLg plasmid encoding the G glycoprotein of the vesicular stomatitis virus. Cell supernatants containing lentiviral particles were collected 72 h after transfection, filtered and subjected to ultracentrifugation. The pellets were resuspended, divided into aliquots and stored at -80°C. To calculate the titer of lentiviral particles, cortical neurons were seeded in a 24-well plate and infected at 5 DIV with serial dilutions (10⁻³ to 10⁻⁷) of lentiviral particles overexpressing tRFP-TDP-43(wt), tRFP-TDP-43(A315T) and tRFP. Uninfected cortical neurons were used as controls. The experiment was repeated in triplicate for each condition. Cortical neurons were fixed after 9 days *in vitro* (DIV) and processed for immunofluorescence with tRFP and TuJ1 primary antibodies. ArrayScan microscope (Thermo Fisher ArrayScan XTI HCA Reader) was used to acquire 20 random fields/well. For every field we counted tRFP-positive infected cells (red) and the total number of cells, stained with a nuclear marker (DAPI). A ratio of total tRFP-positive cells to DAPI-positive cells was calculated for each well. To calculate the titer a given ratio of tRFP-positive cells to total DAPI positive cells between 0.1% and 10% (dynamic range) was chosen, and this formula was used: (Infected cells/Total cells) *Dilution factor *Number of seeded cells. In our experiments a multiplicity of infection (MOI)=4 was used to achieve the transduction of most cells (average >96%, see [Figure 1A'](#)), without detectable cellular toxicity. Cortical neurons were infected at 5 DIV and treated, fixed or lysed at different DIV based on the experimental needs.

Immunofluorescence

Cells were fixed with 4% Paraformaldehyde (PFA)/4% Sucrose in 1X PBS for 15 min, then incubated with primary antibodies in 10% Goat

Serum (GS), 0.1% Triton in 1X PBS overnight at 4°C. For antibodies directed against nuclear epitopes a permeabilization step of 10 min with 0.5% Triton in 1X PBS was added. Subsequently, cells were incubated with secondary antibodies, washed three times with 1X PBS and counterstained with DAPI (D9542, Sigma). Images were acquired using Leica Confocal SP8 (Leica TCS SP8 SMD FLIM Laser scanning Confocal), Nikon Spinning Disk (Nikon CSU-X1 Spinning Disk, Nikon TE2 inverted microscope), Axio Observer (Zeiss Axio Observer.Z1 with Hamamatsu EM9100). The quantification of all experiments was performed with the NIS-element Software (Nikon). When IF analyses were combined with heat shock treatments, cortical neurons were seeded in 24-well plates and infected as usual. At 14 DIV the plates were incubated in a water bath at 43°C for 60 min, washed in 1X D-PBS and processed for immunofluorescence.

Western blotting

Cortical neurons were scraped at room temperature using 50 μL of Lysis Buffer (5% SDS, 10 mM EDTA, 50 mM Hepes pH 7.4) with the addition of protease inhibitors (Leupeptin, Sigma, L2884; Aprotinin, Sigma, A1153; PMSF, Sigma, P7626; Pepstatin A, Sigma, P5318; Sodium Orthovanadate, Sigma, S6508; Sodium Pyrophosphate, Sigma, 221,368; Sodium Fluoride Sigma, S6776; β-Glycerophosphate Sigma, G6251). All protein extracts were sonicated and quantified with Pierce™ BCA Protein Assay kit (ThermoFisher, 23225). 25 μg protein lysate were resuspended in Laemmli buffer 1X (Sigma, S3401-1VL), denatured at 95°C for 5 min and loaded onto a polyacrylamide gel (Mini-PROTEAN(R) TGX™ Precast Gels 4%–20%, Biorad, 456-1094). Proteins were transferred to a nitrocellulose membrane (Biorad, 1704,159) using Trans-Blot(R) Turbo™ (Biorad). Membranes were incubated in blocking buffer (5% milk in TTBS) for 1 h at RT, then overnight at 4°C with primary antibodies diluted in blocking buffer. The membranes were incubated with secondary antibodies in blocking buffer. Bands were revealed using the Clarity™ Western ECL Substrate (Biorad, 170-5061). The images were acquired using the ChemiDoc™MP (Biorad) and the quantification was performed with Image Lab™Software (Biorad).

Primary and secondary antibodies

See [Supplemental Table 2](#).

Subcellular fractionation

All described procedures were performed at 4°C. Cortical neurons were washed in 1xPBS, scraped and lysed for 10 min in Lysis Buffer (50 mM Tris-HCl pH 8.0, 10 mM NaCl, 5 mM MgCl₂, 0.1% Nonidet P-40) with the addition of protease inhibitors. The lysate was spun at 1,000 × g for 15 min to pellet the nuclear fraction (P1). The supernatant (S1) was centrifuged at 50,000 rpm for 60 min in a TLA55 rotor (Beckman) to yield crude cytosol (S2) and crude membrane pellet (P2). The pellet (P2) was resuspended in Lysis buffer without Nonidet P-40 and centrifuged again at 50,000 rpm for 60 min to yield washed crude membrane pellet (P2'). The nuclear fraction (P1) was washed three times with Lysis buffer without Nonidet P-40 at 1,000 × g for 15 min. Pellet was resuspended in a high-salt buffer (20 mM HEPES pH 7.5,

0.5 M NaCl, 1 mM EDTA, 1 mM dithiothreitol and protease inhibitors) and rotated for 20 min. The pellet was centrifuged at 17,700 g for 30 min and the supernatant, containing the nuclear extract, was collected.

Puromycylation assay

DIV 14 cortical neurons plated on microfluidic chambers were treated with 2 μ M puromycin (Sigma, P8833) for 5 min. Pulse-labeling with a low concentration of puromycin, a structural analog of aminoacyl-tRNAs that is incorporated by nascent polypeptide chains, causing peptide release and disassembly of the two ribosomal subunits, was used as a readout of new protein synthesis (David et al., 2012). After treatment, the cultures were fixed and processed for immunofluorescence using an anti-puromycin primary antibody. Puromycin mean pixel intensity was measured in the soma, in 30 μ m axon shaft and in the growth cone of at least 10 neurons per condition for each experiment.

Colocalization analysis

Colocalization analysis between tRFP-tagged TDP43 and endogenous HuC/D, RPS6 and RPL26 was performed in the soma of DIV 9 cortical neurons, at least 10 neurons per condition for each experiment. Pearson's correlation analysis was carried out using the ImageJ plugin JACoP; thresholds were set as described (Bolte and Cordelières, 2006).

ROS measurement

Cortical neurons, plated in a 96-well plate (Greiner Bio-One, 655090) and cultured up to DIV 13, were loaded with 5 μ M dichlorofluorescein diacetate (CM-H2DCFDA, ThermoFisher, C6827), a probe that turns into a fluorescent molecule (2',7'-dichlorofluorescein, DCF) upon oxidation by intracellular ROS. The CM-H2DCFDA loading was performed in KRH pH 7.4 buffer (125 mM NaCl, 25 mM HEPES/NaOH pH 7.4, 5 mM KCl, 1.2 mM MgCl₂, 2 mM CaCl₂, 6 mM Glucose) for 30 min at 37°C, followed by 10 min of incubation with the nuclear dye 1X Hoechst (Sigma, 33258; Vannocci et al., 2018). For iron overload, neurons were treated with 20 μ M ferric ammonium citrate for 2 days before the analysis (Codazzi et al., 2016). The images were acquired using ArrayScan (ThermoFisher ArrayScan XTI HCA Reader) and the fluorescence intensity analysis was carried out by the ALEMBOC Facility of the San Raffaele Hospital.

Electrophysiology

Individual slides with cortical neuronal cultures were placed in a recording chamber mounted on the stage of an upright BX51WI microscope (Olympus) equipped with differential interference contrast optics (DIC). Cultures were perfused with artificial cerebrospinal fluid (ACSF) containing (in mM): 125 NaCl, 2.5 KCl, 1.25 NaH₂PO₄, 2 CaCl₂, 25 NaHCO₃, 1 MgCl₂, and 11 D-glucose, saturated with 95% O₂ and 5% CO₂ (pH 7.3). ACSF was continuously flowing at a rate of 2–3 mL/min at 32°C. For mEPSC recordings,

ACSF was added with the Na⁺ channel specific blocker tetrodotoxin (TTX, 1 μ M). Whole-cell patch-clamp recordings were performed in cortical neurons using pipettes filled with a solution containing the following (in mM): 124 KH₂PO₄, 10 NaCl, 10 HEPES, 0.5 EGTA, 2 MgCl₂, 2 Na₂-ATP, 0.02 Na-GTP (pH 7.2, adjusted with KOH; tip resistance: 4–6 M Ω). All recordings were performed using a MultiClamp 700B amplifier interfaced with a computer through a Digidata 1440A (Molecular Devices, Sunnyvale, CA, United States). Traces were sampled at a frequency of 10 kHz and low pass filtered at 2 kHz. Data were acquired using Clampex software (Molecular Devices) and analyzed with Clampfit and GraphPad Prism applications. Statistical comparisons were obtained using SigmaStat 3.5 (Systat, San Jose, CA).

Calcium analyses

Cortical neurons were incubated with 4 μ M fura-2 acetoxyethyl ester (AM, Calbiochem, CAS 108964-32-5) 40 min at 37°C; the ratiometric properties of fura-2 (excitation at 340 nm and 380 nm and emission at 510 nm) permit the analysis of intracellular Ca²⁺ levels both at basal conditions and upon stimulation with 100 μ M glutamate. Imaging setup and analysis are the same of FM1-43 assay. Single-cell video imaging setup consists of an Axioskope 2 microscope (Zeiss, Oberkochen, Germany) and a Polychrome IV (Till Photonics, GmbH, Martinsried, Germany) light source. Fluorescence images were collected by a cooled CCD video camera (PCO Computer Optics GmbH, Kelheim, Germany), with a rate of 1 ratio image every 2 s. The "Vision" software (Till Photonics) was used to control the acquisition protocol and to perform data analysis (Codazzi et al., 2006; Rosato et al., 2022).

FM1-43 assay

Neurons were loaded with fura-2AM as previously described, before being subjected to the FM1-43 assay. FM1-43 is a styryl dye whose loading and release from synaptic vesicles provides a reliable measurement of vesicle release. The neurons were treated with 20 μ M FM1-43 (Sigma, cat. SCT126; Betz and Bewick, 1992), dissolved in high K⁺ (60 mM)-containing KRH (HK-KRH; Na⁺ concentration was adjusted to maintain isotonicity), diluted 1:1 in normal KRH to obtain the required final KCl and FM1-43 concentration (30 mM and 10 μ M respectively). FM1-43 was kept in the extracellular solution for 2 min, to complete endocytosis; this step was followed by several washes with dye-free KRH buffer, to eliminate the excess of FM1-43; after an additional stimulation with HK-KRH, fluorescence decay of FM1-43 over time was measured. The imaging setup is the same described for fura-2 calcium assay. FM1-43 fluorescence analyses were performed as described (Lazarenko et al., 2018).

Electron microscopy analysis

Neuronal cultures were fixed with 4% paraformaldehyde (PFA) and 2% (wt/vol.) glutaraldehyde in cacodylate buffer 0.12 mol/L pH 7.4 overnight at 4°C, followed by incubation at room temperature for 2 h in 1% (wt/vol.) OsO₄, 1.5% potassium ferrocyanide in 100 mM

cadodylate buffer pH 7.4 for 1 h on ice. After dehydration in a graded series of ethanol preparations, tissue samples were cleared in propylene oxide, embedded in epoxy medium (Epoxy Embedding Medium kit; Sigma-Aldrich, St. Louis, MO 63103 USA), and polymerized at 60°C for 72 h. From each sample, one semi-thin (1 μ m) section was cut with a Leica EM UC6 ultramicrotome (Leica Microsystems, Vienna, Austria). Ultra-thin (60 nm thick) sections of areas of interest were then obtained, counterstained with uranyl acetate and lead citrate, and examined with a transmission electron microscope (Talos 120C Fei), image were acquired with a 4kx4k Ceta CMOS camera (Thermo Fisher Scientific).

Transcriptome and translome analysis

Miniaturized sucrose gradients were used to isolate free or polysomal RNA from cell bodies and axons of CNs cultured in microfluidic chambers, as described above. The procedure for polysome profiling by miniaturized sucrose gradient fractionation was adapted from published protocols (Negro et al., 2018). The procedure consists of the following steps: (i) wtTDP-43, mutTDP-43 and ctr neurons are plated in microfluidic chambers for 9 DIV; (ii) axonal and cell body compartments of these neurons are lysed and loaded onto a miniaturized sucrose gradient to separate polysome-engaged mRNAs from sub-polysomal mRNAs; (iii) polysomal mRNAs and sub-polysomal mRNA fractions are isolated; (iv) mRNAs are extracted from these fractions and sequenced (see also Supplementary Figure 5).

Sequencing data were retrieved from Gene Expression Omnibus (GEO ID: GSE239419) and processed as described by the authors. Briefly, reads were first preprocessed for adapter removal and trimming, then mapped to the mouse genome (GRCm38.p6, ENSEMBL release 92 and Gencode M17 gene annotation) and finally deduplicated. After sample size normalization based on the trimmed mean of M-values method, only genes with FPKM > 10 in all replicates of at least 1 sample were kept for subsequent analysis. Differentially expressed genes were identified by the edgeR applying multiple thresholds (CPM > 0.05, absolute log₂ fold change > 0.75, value of $p < 0.05$). Annotation enrichment analysis with Gene Ontology terms, REACTOME and KEGG pathways were performed with the clusterProfiler Bioconductor package. GO analysis was performed as described (Bernabo et al., 2017).

Gene ontology tables were searched using the following query words: translation, ribosom* and polysom* for mRNA translation; oxidative, peroxid* and reactive oxygen species for oxidative stress; synap*; vesicle, exocyt*, endocyt* and neurotransmitter for synaptogenesis and synaptic function.

Statistical analysis

All values are expressed as mean \pm standard error of the mean (SEM) of at least 3 independent experiments. Statistical analysis was performed using the GraphPad Prism software for the choice of optimal statistical tests based on data distribution. The statistical tests for each experiment are reported in the figure legends. Differences yielding a p value ≥ 0.05 were regarded as non-significant. With respect to decay curves (Figure 5), we fitted the model fluorescence = $2^{(\alpha_{ctr} + \sum I_i \Delta_i)t} \varepsilon$ where α_{ctr} is the coefficient

for the controls; I_i is the indicatrix functions for experimental condition and Δ_i represents the difference between control and the experimental condition i . ε is supposed to have lognormal distribution.

This model allows an easy interpretation of fluorescence decay because α_{ctr} , $(\alpha_{ctr} + \Delta_{wtTDP-43})$ and $(\alpha_{ctr} + \Delta_{mutTDP-43})$ are related to the fluorescence half-life in the three experimental conditions. Furthermore, multiplicative log-normal distributed errors address for the higher variability observed in correspondence of higher mean values.

Data availability statement

The raw data supporting the conclusions of this article will be made available by the authors, without undue reservation.

Ethics statement

The animal study was approved by: Il Comitato I.A.C.U.C.—Ospedale San Raffaele, Organismo Preposto al Benessere degli Animali. The study was conducted in accordance with the local legislation and institutional requirements.

Author contributions

AP: Conceptualization, Data curation, Investigation, Methodology, Writing – original draft. LC: Conceptualization, Data curation, Investigation, Methodology, Writing – original draft, Formal analysis, Supervision, Validation. FL: Data curation, Formal analysis, Investigation, Methodology, Visualization, Writing – review & editing. CM: Data curation, Investigation, Methodology, Visualization, Writing – review & editing. ES: Investigation, Methodology, Visualization, Writing – review & editing. AA: Data curation, Software, Visualization, Writing – review & editing. PP: Investigation, Methodology, Visualization, Writing – review & editing. MM: Investigation, Methodology, Visualization, Writing – review & editing. FiC: Visualization, Writing – review & editing. OC: Writing – review & editing. ST: Writing – review & editing, Investigation, Methodology, Writing – original draft. AQ: Investigation, Methodology, Data curation, Visualization, Writing – review & editing. J-MC: Investigation, Methodology, Conceptualization, Visualization, Writing – review & editing. GV: Data curation, Methodology, Funding acquisition, Investigation, Visualization, Writing – review & editing. FrC: Data curation, Funding acquisition, Investigation, Methodology, Writing – review & editing, Conceptualization, Formal analysis, Supervision, Validation, Visualization, Writing – original draft. GC: Conceptualization, Data curation, Formal analysis, Funding acquisition, Investigation, Resources, Software, Supervision, Validation, Validation, Writing – original draft, Writing – review & editing.

Funding

This study has been supported by AriSLA (AxRibALS grant to GC and GV) and Ministero della Salute (RF21-2766 to FrC and GC). J-MC and ES are funded by the European Union (ERC Starting Grant, AXONENDO, 851966).

Acknowledgments

The authors thank all members of the GC and GV labs for critical discussion of our data. Thanks to Claudia Rivoletti for preliminary experiments. AP was supported during her PhD studies thanks to a very generous donation by the Fronzaroli family. Image analysis was carried out at ALEMBIC, an advanced microscopy laboratory established by the San Raffaele Scientific Institute and University.

Conflict of interest

The authors declare that the research was conducted in the absence of any commercial or financial relationships that could be construed as a potential conflict of interest.

References

- Alami, N. H., Smith, R. B., Carrasco, M. A., Williams, L. A., Winborn, C. S., Han, S. S., et al. (2014). Axonal transport of TDP-43 mRNA granules is impaired by ALS-causing mutations. *Neuron* 81, 536–543. doi: 10.1016/j.neuron.2013.12.018
- Altman, T., Ionescu, A., Ibraheem, A., Priesmann, D., Gradus-Pery, T., Farberov, L., et al. (2021). Axonal TDP-43 condensates drive neuromuscular junction disruption through inhibition of local synthesis of nuclear encoded mitochondrial proteins. *Nat. Commun.* 12:6914. doi: 10.1038/s41467-021-27221-8
- Aly, A., Laszlo, Z. I., Rajkumar, S., Demir, T., Hindley, N., Lamont, D. J., et al. (2023). Integrative proteomics highlight presynaptic alterations and c-Jun misactivation as convergent pathomechanisms in ALS. *Acta Neuropathol.* 146, 451–475. doi: 10.1007/s00401-023-02611-y
- Amaral, E., Guatimosim, S., and Guatimosim, C. (2011). Using the fluorescent styryl dye FM1-43 to visualize synaptic vesicles exocytosis and endocytosis in motor nerve terminals. *Methods Mol. Biol.* 689, 137–148. doi: 10.1007/978-1-60761-950-5_8
- Amendola, M., Venneri, M. A., Biffi, A., Vigna, E., and Naldini, L. (2005). Coordinate dual-gene transgenesis by lentiviral vectors carrying synthetic bidirectional promoters. *Nat. Biotechnol.* 23, 108–116. doi: 10.1038/nbt1049
- Arai, T., Hasegawa, M., Akiyama, H., Ikeda, K., Nonaka, T., Mori, H., et al. (2006). TDP-43 is a component of ubiquitin-positive tau-negative inclusions in frontotemporal lobar degeneration and amyotrophic lateral sclerosis. *Biochem. Biophys. Res. Commun.* 351, 602–611. doi: 10.1016/j.bbrc.2006.10.093
- Avendano-Vazquez, S. E., Dhir, A., Bembich, S., Buratti, E., Proudfoot, N., and Baralle, F. E. (2012). Autoregulation of TDP-43 mRNA levels involves interplay between transcription, splicing, and alternative polyA site selection. *Genes Dev.* 26, 1679–1684. doi: 10.1101/gad.194829.112
- Ayala, Y. M., De Conti, L., Avendano-Vazquez, S. E., Dhir, A., Romano, M., D'Ambrogio, A., et al. (2011). TDP-43 regulates its mRNA levels through a negative feedback loop. *EMBO J.* 30, 277–288. doi: 10.1038/emboj.2010.310
- Ayala, Y. M., Pantano, S., D'Ambrogio, A., Buratti, E., Brindisi, A., Marchetti, C., et al. (2005). Human, drosophila, and C. elegans TDP43: nucleic acid binding properties and splicing regulatory function. *J. Mol. Biol.* 348, 575–588. doi: 10.1016/j.jmb.2005.02.038
- Ayala, Y. M., Zago, P., D'Ambrogio, A., Xu, Y. F., Petrucelli, L., Buratti, E., et al. (2008). Structural determinants of the cellular localization and shuttling of TDP-43. *J. Cell Sci.* 121, 3778–3785. doi: 10.1242/jcs.038950
- Barber, S. C., and Shaw, P. J. (2010). Oxidative stress in ALS: key role in motor neuron injury and therapeutic target. *Free Radic. Biol. Med.* 48, 629–641. doi: 10.1016/j.freeradbiomed.2009.11.018
- Bedogni, F., Hodge, R. D., Elsen, G. E., Nelson, B. R., Daza, R. A., Beyer, R. P., et al. (2010). Tbr1 regulates regional and laminar identity of postmitotic neurons in developing neocortex. *Proc. Natl. Acad. Sci. U. S. A.* 107, 13129–13134. doi: 10.1073/pnas.1002285107
- Beers, D. R., Henkel, J. S., Xiao, Q., Zhao, W., Wang, J., Yen, A. A., et al. (2006). Wild-type microglia extend survival in PU.1 knockout mice with familial amyotrophic lateral sclerosis. *Proc. Natl. Acad. Sci. U. S. A.* 103, 16021–16026. doi: 10.1073/pnas.0607423103
- Bernabo, P., Tebaldi, T., Groen, E. J. N., Lane, F. M., Perenthaler, E., Mattedi, F., et al. (2017). In vivo Translatome profiling in spinal muscular atrophy reveals a role for SMN protein in ribosome biology. *Cell Rep.* 21, 953–965. doi: 10.1016/j.celrep.2017.10.010
- Bettagazzi, B., Pelizzoni, I., Salerno Scarzella, F., Restelli, L. M., Zacchetti, D., Maltecca, F., et al. (2019). Upregulation of Peroxiredoxin 3 protects Aβ312-KO cortical

Publisher's note

All claims expressed in this article are solely those of the authors and do not necessarily represent those of their affiliated organizations, or those of the publisher, the editors and the reviewers. Any product that may be evaluated in this article, or claim that may be made by its manufacturer, is not guaranteed or endorsed by the publisher.

Supplementary material

The Supplementary material for this article can be found online at: <https://www.frontiersin.org/articles/10.3389/fncel.2023.1253543/full#supplementary-material>

neurons in vitro from oxidative stress: a paradigm for neuronal cell survival under neurodegenerative conditions. *Oxid. Med. Cell. Longev.* 2019:4721950. doi: 10.1155/2019/4721950

Betz, W. J., and Bewick, G. S. (1992). Optical analysis of synaptic vesicle recycling at the frog neuromuscular junction. *Science* 255, 200–203. doi: 10.1126/science.1553547

Bhattarai, A., Chen, Z., Ward, P. G. D., Talman, P., Mathers, S., Phan, T. G., et al. (2020). Serial assessment of iron in the motor cortex in limb-onset amyotrophic lateral sclerosis using quantitative susceptibility mapping. *Quant. Imaging Med. Surg.* 10, 1465–1476. doi: 10.21037/qims-20-187

Blair, I. P., Williams, K. L., Warraich, S. T., Durnall, J. C., Thoeng, A. D., Manavis, J., et al. (2010). FUS mutations in amyotrophic lateral sclerosis: clinical, pathological, neurophysiological and genetic analysis. *J. Neurol. Neurosurg. Psychiatry* 81, 639–645. doi: 10.1136/jnnp.2009.194399

Bolte, S., and Cordelières, F. P. (2006). A guided tour into subcellular colocalization analysis in light microscopy. *J. Microsc.* 224, 213–232. doi: 10.1111/j.1365-2818.2006.01706.x

Briese, M., Saal-Bauernschubert, L., Luningschror, P., Moradi, M., Dombert, B., Surrey, V., et al. (2020). Loss of Tdp-43 disrupts the axonal transcriptome of motoneurons accompanied by impaired axonal translation and mitochondria function. *Acta Neuropathol. Commun.* 8:116. doi: 10.1186/s40478-020-00987-6

Brown, R. H., and Al-Chalabi, A. (2017). Amyotrophic lateral sclerosis. *N. Engl. J. Med.* 377:1602. doi: 10.1056/NEJMc1710379

Brown, A. L., Wilkins, O. G., Keuss, M. J., Hill, S. E., Zanovello, M., Lee, W. C., et al. (2022). TDP-43 loss and ALS-risk SNPs drive mis-splicing and depletion of UNC13A. *Nature* 603, 131–137. doi: 10.1038/s41586-022-04436-3

Buratti, E. (2015). Functional significance of TDP-43 mutations in disease. *Adv. Genet.* 91, 1–53. doi: 10.1016/bs.adgen.2015.07.001

Buratti, E., Dork, T., Zuccato, E., Pagani, F., Romano, M., and Baralle, F. E. (2001). Nuclear factor TDP-43 and SR proteins promote in vitro and in vivo CFTR exon 9 skipping. *EMBO J.* 20, 1774–1784. doi: 10.1093/emboj/20.7.1774

Chu, J. F., Majumder, P., Chatterjee, B., Huang, S. L., and Shen, C. J. (2019). TDP-43 regulates coupled dendritic mRNA transport-translation processes in co-operation with FMRP and Staufen1. *Cell Rep.* 29, 3118–3133 e3116. doi: 10.1016/j.celrep.2019.10.061

Codazzi, F., Di Cesare, A., Chiulli, N., Albanese, A., Meyer, T., Zacchetti, D., et al. (2006). Synergistic control of protein kinase Cgamma activity by ionotropic and metabotropic glutamate receptor inputs in hippocampal neurons. *J. Neurosci.* 26, 3404–3411. doi: 10.1523/JNEUROSCI.0478-06.2006

Codazzi, F., Hu, A., Rai, M., Donatello, S., Salerno Scarzella, F., Mangiameli, E., et al. (2016). Friedreich ataxia-induced pluripotent stem cell-derived neurons show a cellular phenotype that is corrected by a benzamide HDAC inhibitor. *Hum. Mol. Genet.* 25, 4847–4855. doi: 10.1093/hmg/ddw308

Cohen, T. J., Lee, V. M., and Trojanowski, J. Q. (2011). TDP-43 functions and pathogenic mechanisms implicated in TDP-43 proteinopathies. *Trends Mol. Med.* 17, 659–667. doi: 10.1016/j.molmed.2011.06.004

Colombrita, C., Onesto, E., Megiorni, F., Pizzuti, A., Baralle, F. E., Buratti, E., et al. (2012). TDP-43 and FUS RNA-binding proteins bind distinct sets of cytoplasmic messenger RNAs and differently regulate their post-transcriptional fate in motoneuron-like cells. *J. Biol. Chem.* 287, 15635–15647. doi: 10.1074/jbc.M111.333450

- Colombrita, C., Zennaro, E., Fallini, C., Weber, M., Sommacal, A., Buratti, E., et al. (2009). TDP-43 is recruited to stress granules in conditions of oxidative insult. *J. Neurochem.* 111, 1051–1061. doi: 10.1111/j.1471-4159.2009.06383.x
- Conicella, A. E., Zerze, G. H., Mittal, J., and Fawzi, N. L. (2016). ALS mutations disrupt phase separation mediated by alpha-helical structure in the TDP-43 low-complexity C-terminal domain. *Structure* 24, 1537–1549. doi: 10.1016/j.str.2016.07.007
- Cosker, K. E., Fenstermacher, S. J., Pazyra-Murphy, M. F., Elliott, H. L., and Segal, R. A. (2016). The RNA-binding protein SFPQ orchestrates an RNA regulon to promote axon viability. *Nat. Neurosci.* 19, 690–696. doi: 10.1038/nn.4280
- Costessi, L., Porro, F., Iaconig, A., and Muro, A. F. (2014). TDP-43 regulates beta-adducin (Add2) transcript stability. *RNA Biol.* 11, 1280–1290. doi: 10.1080/15476286.2014.996081
- Cremona, O., Di Paolo, G., Wenk, M. R., Luthi, A., Kim, W. T., Takei, K., et al. (1999). Essential role of phosphoinositide metabolism in synaptic vesicle recycling. *Cells* 99, 179–188. doi: 10.1016/s0092-8674(00)81649-9
- David, A., Dolan, B., Hickman, H., Knowlton, J., Clavarino, G., Pierre, P., et al. (2012). Nuclear translation visualized by ribosome-bound nascent chain puromycylation. *J. Cell Biol.* 197, 45–57. doi: 10.1083/jcb.201112145
- de Boer, E. M. J., Orié, V. K., Williams, T., Baker, M. R., De Oliveira, H. M., Polvikoski, T., et al. (2020). TDP-43 proteinopathies: a new wave of neurodegenerative diseases. *J. Neurol. Neurosurg. Psychiatry* 92, 86–95. doi: 10.1136/jnnp-2020-322983
- Devlin, A. C., Burr, K., Borooah, S., Foster, J. D., Cleary, E. M., Geti, I., et al. (2015). Human iPSC-derived motoneurons harbouring TARDBP or C9ORF72 ALS mutations are dysfunctional despite maintaining viability. *Nat. Commun.* 6:5999. doi: 10.1038/ncomms6999
- Dewey, C. M., Cenik, B., Sephton, C. F., Johnson, B. A., Herz, J., and Yu, G. (2012). TDP-43 aggregation in neurodegeneration: are stress granules the key? *Brain Res.* 1462, 16–25. doi: 10.1016/j.brainres.2012.02.032
- Diaz-Garcia, S., Ko, V. I., Vazquez-Sanchez, S., Chia, R., Arogundade, O. A., Rodriguez, M. J., et al. (2021). Nuclear depletion of RNA-binding protein ELAVL3 (HuC) in sporadic and familial amyotrophic lateral sclerosis. *Acta Neuropathol.* 142, 985–1001. doi: 10.1007/s00401-021-02374-4
- Ederle, H., Funk, C., Abou-Ajram, C., Hutten, S., Funk, E. B. E., Kehlenbach, R. H., et al. (2018). Nuclear egress of TDP-43 and FUS occurs independently of Exportin-1/CRM1. *Sci. Rep.* 8:7084. doi: 10.1038/s41598-018-25007-5
- Einhauer, A., and Jungbauer, A. (2001). The FLAG peptide, a versatile fusion tag for the purification of recombinant proteins. *J. Biochem. Biophys. Methods* 49, 455–465. doi: 10.1016/s0165-022x(01)00213-5
- Fallini, C., Bassell, G. J., and Rossoll, W. (2012). The ALS disease protein TDP-43 is actively transported in motor neuron axons and regulates axon outgrowth. *Hum. Mol. Genet.* 21, 3703–3718. doi: 10.1093/hmg/dds205
- Fischer, L. R., Culver, D. G., Tennant, P., Davis, A. A., Wang, M., Castellano-Sanchez, A., et al. (2004). Amyotrophic lateral sclerosis is a distal axonopathy: evidence in mice and man. *Exp. Neurol.* 185, 232–240. doi: 10.1016/j.expneurol.2003.10.004
- Fogarty, M. J. (2019). Amyotrophic lateral sclerosis as a synaptopathy. *Neural Regen. Res.* 14, 189–192. doi: 10.4103/1673-5374.244782
- Fogarty, M. J., Kanjhan, R., Bellingham, M. C., and Noakes, P. G. (2016a). Glycinergic neurotransmission: a potent regulator of embryonic motor neuron dendritic morphology and synaptic plasticity. *J. Neurosci.* 36, 80–87. doi: 10.1523/JNEUROSCI.1576-15.2016
- Fogarty, M. J., Mu, E. W. H., Lavidis, N. A., Noakes, P. G., and Bellingham, M. C. (2017). Motor areas show altered dendritic structure in an amyotrophic lateral sclerosis mouse model. *Front. Neurosci.* 11:609. doi: 10.3389/fnins.2017.00609
- Fogarty, M. J., Mu, E. W., Noakes, P. G., Lavidis, N. A., and Bellingham, M. C. (2016b). Marked changes in dendritic structure and spine density precede significant neuronal death in vulnerable cortical pyramidal neuron populations in the SOD1(G93A) mouse model of amyotrophic lateral sclerosis. *Acta Neuropathol. Commun.* 4:77. doi: 10.1186/s40478-016-0347-y
- Fratta, P., Sivakumar, P., Humphrey, J., Lo, K., Ricketts, T., Oliveira, H., et al. (2018). Mice with endogenous TDP-43 mutations exhibit gain of splicing function and characteristics of amyotrophic lateral sclerosis. *EMBO J.* 37:e98684. doi: 10.15252/embj.201798684
- Fusco, C. M., Desch, K., Dorrabaum, A. R., Wang, M., Staab, A., Chan, I. C. W., et al. (2021). Neuronal ribosomes exhibit dynamic and context-dependent exchange of ribosomal proteins. *Nat. Commun.* 12:6127. doi: 10.1038/s41467-021-26365-x
- Genc, B., Jara, J. H., Schultz, M. C., Manuel, M., Stanford, M. J., Gautam, M., et al. (2016). Absence of UCHL1 function leads to selective motor neuropathy. *Ann. Clin. Transl. Neurol.* 3, 331–345. doi: 10.1002/acn3.298
- Gil, J., Funalot, B., Verschuere, A., Danel-Brunaud, V., Camu, W., Vandenberghe, N., et al. (2008). Causes of death amongst French patients with amyotrophic lateral sclerosis: a prospective study. *Eur. J. Neurol.* 15, 1245–1251. doi: 10.1111/j.1468-1331.2008.02307.x
- Gitcho, M. A., Baloh, R. H., Chakraverty, S., Mayo, K., Norton, J. B., Levitch, D., et al. (2008). TDP-43 A315T mutation in familial motor neuron disease. *Ann. Neurol.* 63, 535–538. doi: 10.1002/ana.21344
- Guatteo, E., Carunchio, I., Pieri, M., Albo, F., Canu, N., Mercuri, N. B., et al. (2007). Altered calcium homeostasis in motor neurons following AMPA receptor but not voltage-dependent calcium channels' activation in a genetic model of amyotrophic lateral sclerosis. *Neurobiol. Dis.* 28, 90–100. doi: 10.1016/j.nbd.2007.07.002
- Guo, W., Naujock, M., Fumagalli, L., Vandorine, T., Baatsen, P., Boon, R., et al. (2017). HDAC6 inhibition reverses axonal transport defects in motor neurons derived from FUS-ALS patients. *Nat. Commun.* 8:861. doi: 10.1038/s41467-017-00911-y
- Guo, W., Stoklund Dittlau, K., and Van Den Bosch, L. (2020). Axonal transport defects and neurodegeneration: molecular mechanisms and therapeutic implications. *Semin. Cell Dev. Biol.* 99, 133–150. doi: 10.1016/j.semcdb.2019.07.010
- Handley, E. E., Pitman, K. A., Dawkins, E., Young, K. M., Clark, R. M., Jiang, T. C., et al. (2017). Synapse dysfunction of layer V pyramidal neurons precedes neurodegeneration in a mouse model of TDP-43 Proteinopathies. *Cereb. Cortex* 27, 3630–3647. doi: 10.1093/cercor/bhw185
- Hardiman, O., Al-Chalabi, A., Chio, A., Corr, E. M., Logroscino, G., Robberecht, W., et al. (2017). Amyotrophic lateral sclerosis. *Nat. Rev. Dis. Primers.* 3:17085. doi: 10.1038/nrdp.2017.85
- Harrison, A. F., and Shorter, J. (2017). RNA-binding proteins with prion-like domains in health and disease. *Biochem. J.* 474, 1417–1438. doi: 10.1042/BCJ20160499
- Helmchen, F., Svoboda, K., Denk, W., and Tank, D. W. (1999). In vivo dendritic calcium dynamics in deep-layer cortical pyramidal neurons. *Nat. Neurosci.* 2, 989–996. doi: 10.1038/14788
- Higashi, S., Kabuta, T., Nagai, Y., Tsuchiya, Y., Akiyama, H., and Wada, K. (2013). TDP-43 associates with stalled ribosomes and contributes to cell survival during cellular stress. *J. Neurochem.* 126, 288–300. doi: 10.1111/jnc.12194
- Igatz, L. M., Kwong, L. K., Lee, E. B., Chen-Plotkin, A., Swanson, E., Unger, T., et al. (2011). Dysregulation of the ALS-associated gene TDP-43 leads to neuronal death and degeneration in mice. *J. Clin. Invest.* 121, 726–738. doi: 10.1172/JCI44867
- Jensen, B. K., Schuldi, M. H., McAvoy, K., Russell, K. A., Boehringer, A., Curran, B. M., et al. (2020). Synaptic dysfunction induced by glycine-alanine dipeptides in C9orf72-ALS/FTD is rescued by SV2 replenishment. *EMBO Mol. Med.* 12:e10722. doi: 10.15252/emmm.201910722
- Jiang, M. C., Adimula, A., Birch, D., and Heckman, C. J. (2017). Hyperexcitability in synaptic and firing activities of spinal motoneurons in an adult mouse model of amyotrophic lateral sclerosis. *Neuroscience* 362, 33–46. doi: 10.1016/j.neuroscience.2017.08.041
- Jung, H., Yoon, B. C., and Holt, C. E. (2012). Axonal mRNA localization and local protein synthesis in nervous system assembly, maintenance and repair. *Nat. Rev. Neurosci.* 13, 308–324. doi: 10.1038/nrn3210
- Kato, S., Kato, M., Abe, Y., Matsumura, T., Nishino, T., Aoki, M., et al. (2005). Redox system expression in the motor neurons in amyotrophic lateral sclerosis (ALS): immunohistochemical studies on sporadic ALS, superoxide dismutase 1 (SOD1)-mutated familial ALS, and SOD1-mutated ALS animal models. *Acta Neuropathol.* 110, 101–112. doi: 10.1007/s00401-005-1019-3
- Kato, S., Saeki, Y., Aoki, M., Nagai, M., Ishigaki, A., Itoyama, Y., et al. (2004). Histological evidence of redox system breakdown caused by superoxide dismutase 1 (SOD1) aggregation is common to SOD1-mutated motor neurons in humans and animal models. *Acta Neuropathol.* 107, 149–158. doi: 10.1007/s00401-003-0791-1
- Kim, E., and Jung, H. (2020). Local mRNA translation in long-term maintenance of axon health and function. *Curr. Opin. Neurobiol.* 63, 15–22. doi: 10.1016/j.conb.2020.01.006
- Kraemer, B. C., Schuck, T., Wheeler, J. M., Robinson, L. C., Trojanowski, J. Q., Lee, V. M., et al. (2010). Loss of murine TDP-43 disrupts motor function and plays an essential role in embryogenesis. *Acta Neuropathol.* 119, 409–419. doi: 10.1007/s00401-010-0659-0
- Krishnamurthy, K., and Pasinelli, P. (2021). Synaptic dysfunction in amyotrophic lateral sclerosis/frontotemporal dementia: therapeutic strategies and novel biomarkers. *J. Neurosci. Res.* 99, 1499–1503. doi: 10.1002/jnr.24824
- Larkum, M. E., Zhu, J. J., and Sakmann, B. (1999). A new cellular mechanism for coupling inputs arriving at different cortical layers. *Nature* 398, 338–341. doi: 10.1038/18686
- Lazarenko, R. M., DelBove, C. E., and Zhang, Q. (2018). Fluorescent measurement of synaptic activity using FM dyes in dissociated hippocampal cultured neurons. *Bio Protoc* 8:e2690. doi: 10.21203/BioProtoc.2690
- Lee, S. J., Oses-Prieto, J. A., Kawaguchi, R., Sahoo, P. K., Kar, A. N., Rozenbaum, M., et al. (2018). hnRNPs interacting with mRNA localization motifs define axonal RNA regulons. *Mol. Cell. Proteomics* 17, 2091–2106. doi: 10.1074/mcp.RA118.000603
- Lehmkuhl, E. M., Loganathan, S., Alsop, E., Blythe, A. D., Kovalik, T., Mortimore, N. P., et al. (2021). TDP-43 proteinopathy alters the ribosome association of multiple mRNAs including the glypican dally-like protein (Dlp)/GPC6. *Acta Neuropathol. Commun.* 9:52. doi: 10.1186/s40478-021-01148-z
- Liao, B., Zhao, W., Beers, D. R., Henkel, J. S., and Appel, S. H. (2012). Transformation from a neuroprotective to a neurotoxic microglial phenotype in a mouse model of ALS. *Exp. Neurol.* 237, 147–152. doi: 10.1016/j.expneurol.2012.06.011
- Limone, F., Mordes, D., Couto, A., Pietiläinen, O., Joseph, B. J., Burberry, A., et al. (2021). Single-nucleus sequencing reveals enriched expression of genetic risk factors sensitises motor neurons to degeneration in ALS. *bioRxiv [Preprint]*, 1–9.

- Ling, S. C., Polymenidou, M., and Cleveland, D. W. (2013). Converging mechanisms in ALS and FTD: disrupted RNA and protein homeostasis. *Neuron* 79, 416–438. doi: 10.1016/j.neuron.2013.07.033
- Liu, J., Su, G., Gao, J., Tian, Y., Liu, X., and Zhang, Z. (2020). Effects of Peroxiredoxin 2 in neurological disorders: a review of its molecular mechanisms. *Neurochem. Res.* 45, 720–730. doi: 10.1007/s11064-020-02971-x
- Liu, J., and Wang, F. (2017). Role of Neuroinflammation in amyotrophic lateral sclerosis: cellular mechanisms and therapeutic implications. *Front. Immunol.* 8:1005. doi: 10.3389/fimmu.2017.01005
- Mackenzie, I. R., Neumann, M., Baborie, A., Sampathu, D. M., Du Plessis, D., Jaros, E., et al. (2011). A harmonized classification system for FTLTD-TDP pathology. *Acta Neuropathol.* 122, 111–113. doi: 10.1007/s00401-011-0845-8
- Mani, M., Lee, S. Y., Lucast, L., Cremona, O., Di Paolo, G., De Camilli, P., et al. (2007). The dual phosphatase activity of synaptojanin1 is required for both efficient synaptic vesicle endocytosis and reavailability at nerve terminals. *Neuron* 56, 1004–1018. doi: 10.1016/j.neuron.2007.10.032
- Marchetto, M. C., Muotri, A. R., Mu, Y., Smith, A. M., Cezar, G. G., and Gage, F. H. (2008). Non-cell-autonomous effect of human SOD1 G37R astrocytes on motor neurons derived from human embryonic stem cells. *Cell Stem Cell* 3, 649–657. doi: 10.1016/j.stem.2008.10.001
- Martinez, J. C., Randolph, L. K., Iacono, D. M., Pernice, H. F., Polleux, F., and Hengst, U. (2019). Pum2 shapes the transcriptome in developing axons through retention of target mRNAs in the cell body. *Neuron* 104, 931–946 e935. doi: 10.1016/j.neuron.2019.08.035
- Matsuki, H., Takahashi, M., Higuchi, M., Makokha, G. N., Oie, M., and Fujii, M. (2013). Both G3BP1 and G3BP2 contribute to stress granule formation. *Genes Cells* 18, 135–146. doi: 10.1111/gtc.12023
- Miller, S. E., Mathiasen, S., Bright, N. A., Pierre, F., Kelly, B. T., Kladt, N., et al. (2015). CALM regulates clathrin-coated vesicle size and maturation by directly sensing and driving membrane curvature. *Dev. Cell* 33, 163–175. doi: 10.1016/j.devcel.2015.03.002
- Mitani, T. T., Beck, G., Kido, K., Yamashita, R., Yonenobu, Y., Ogawa, T., et al. (2021). Amyotrophic lateral sclerosis with speech apraxia, predominant upper motor neuron signs, and prominent iron accumulation in the frontal operculum and precentral gyrus. *Neuropathology* 41, 324–331. doi: 10.1111/neup.12763
- Moloney, E. B., de Winter, F., and Verhaagen, J. (2014). ALS as a distal axonopathy: molecular mechanisms affecting neuromuscular junction stability in the presymptomatic stages of the disease. *Front. Neurosci.* 8:252. doi: 10.3389/fnins.2014.00252
- Molyneux, B. J., Arlotta, P., Menezes, J. R., and Macklis, J. D. (2007). Neuronal subtype specification in the cerebral cortex. *Nat. Rev. Neurosci.* 8, 427–437. doi: 10.1038/nrn2151
- Nagano, S., Jinno, J., Abdelhamid, R. F., Jin, Y., Shibata, M., Watanabe, S., et al. (2020). TDP-43 transports ribosomal protein mRNA to regulate axonal translation in neuronal axons. *Acta Neuropathol.* 140, 695–713. doi: 10.1007/s00401-020-02205-y
- Naujock, M., Stanslowsky, N., Bufler, S., Naumann, M., Reinhardt, P., Sternecker, J., et al. (2016). 4-Aminopyridine induced activity rescues Hypoexcitable motor neurons from amyotrophic lateral sclerosis patient-derived induced pluripotent stem cells. *Stem Cells* 34, 1563–1575. doi: 10.1002/stem.2354
- Naumann, M., Pal, A., Goswami, A., Lojewski, X., Japtok, J., Vehlou, A., et al. (2018). Impaired DNA damage response signaling by FUS-NLS mutations leads to neurodegeneration and FUS aggregate formation. *Nat. Commun.* 9:335. doi: 10.1038/s41467-017-02299-1
- Negro, S., Stazi, M., Marchioretto, M., Tebaldi, T., Rodella, U., Duregotti, E., et al. (2018). Hydrogen peroxide is a neuronal alarmin that triggers specific RNAs, local translation of Annexin A2, and cytoskeletal remodeling in Schwann cells. *RNA* 24, 915–925. doi: 10.1261/rna.064816.117
- Neumann, M. (2009). Molecular neuropathology of TDP-43 proteinopathies. *Int. J. Mol. Sci.* 10, 232–246. doi: 10.3390/ijms10010232
- Neumann, M., Sampathu, D. M., Kwong, L. K., Truax, A. C., Micsenyi, M. C., Chou, T. T., et al. (2006). Ubiquitinated TDP-43 in frontotemporal lobar degeneration and amyotrophic lateral sclerosis. *Science* 314, 130–133. doi: 10.1126/science.1134108
- Niedermeier, S., Murn, M., and Choi, P. J. (2019). Respiratory failure in amyotrophic lateral sclerosis. *Chest* 155, 401–408. doi: 10.1016/j.chest.2018.06.035
- Ostroff, L. E., Santini, E., Sears, R., Deane, Z., Kanadia, R. N., LeDoux, J. E., et al. (2019). Axon TRAP reveals learning-associated alterations in cortical axonal mRNAs in the lateral amygdala. *Elife* 8:e51607. doi: 10.7554/eLife.51607
- Pelizzoni, I., Macco, R., Zacchetti, D., Grohovaz, F., and Codazzi, F. (2008). Iron and calcium in the central nervous system: a close relationship in health and sickness. *Biochem. Soc. Trans.* 36, 1309–1312. doi: 10.1042/BST0361309
- Perkins, E. M., Burr, K., Banerjee, P., Mehta, A. R., Dando, O., Selvaraj, B. T., et al. (2021). Altered network properties in C9ORF72 repeat expansion cortical neurons are due to synaptic dysfunction. *Mol. Neurodegener.* 16:13. doi: 10.1186/s13024-021-00433-8
- Pharaoh, G., Sataranatarajan, K., Street, K., Hill, S., Gregston, J., Ahn, B., et al. (2019). Metabolic and stress response changes precede disease onset in the spinal cord of mutant SOD1 ALS mice. *Front. Neurosci.* 13:487. doi: 10.3389/fnins.2019.00487
- Polymenidou, M., Lagier-Tourenne, C., Hutt, K. R., Huelga, S. C., Moran, J., Liang, T. Y., et al. (2011). Long pre-mRNA depletion and RNA missplicing contribute to neuronal vulnerability from loss of TDP-43. *Nat. Neurosci.* 14, 459–468. doi: 10.1038/nn.2779
- Prasad, A., Bharathi, V., Sivalingam, V., Girdhar, A., and Patel, B. K. (2019). Molecular mechanisms of TDP-43 Misfolding and pathology in amyotrophic lateral sclerosis. *Front. Mol. Neurosci.* 12:25. doi: 10.3389/fnmol.2019.00025
- Ragagnin, A. M. G., Shadfar, S., Vidal, M., Jamali, M. S., and Atkin, J. D. (2019). Motor neuron susceptibility in ALS/FTD. *Front. Neurosci.* 13:532. doi: 10.3389/fnins.2019.00532
- Rosato, C., Bettgazzi, B., Intagliata, P., Balbontin Arenas, M., Zacchetti, D., Lanati, A., et al. (2022). Redox and calcium alterations of a Muller cell line exposed to diabetic retinopathy-like environment. *Front. Cell. Neurosci.* 16:862325. doi: 10.3389/fncel.2022.862325
- Roy, S. (2020). Finding order in slow axonal transport. *Curr. Opin. Neurobiol.* 63, 87–94. doi: 10.1016/j.conb.2020.03.015
- Sambri, I., Massa, F., Gullo, F., Meneghini, S., Cassina, L., Carraro, M., et al. (2020). Impaired flickering of the permeability transition pore causes SPG7 spastic paraplegia. *EBioMedicine* 61:103050. doi: 10.1016/j.ebiom.2020.103050
- Sareen, D., O'Rourke, J. G., Meera, P., Muhammad, A. K., Grant, S., Simpkinson, M., et al. (2013). Targeting RNA foci in iPSC-derived motor neurons from ALS patients with a C9ORF72 repeat expansion. *Sci. Transl. Med.* 5:208ra149. doi: 10.1126/scitranslmed.3007529
- Shigeoka, T., Jung, H., Jung, J., Turner-Bridger, B., Ohk, J., Lin, J., et al. (2016). Dynamic axonal translation in developing and mature visual circuits. *Cells* 166, 181–192. doi: 10.1016/j.cell.2016.05.029
- Shigeoka, T., Koppers, M., Wong, H. H., Lin, J. Q., Cagnetta, R., Dwivedy, A., et al. (2019). On-site ribosome Remodeling by locally synthesized ribosomal proteins in axons. *Cell Rep.* 29, 3605–3619 e3610. doi: 10.1016/j.celrep.2019.11.025
- Sidibé, H., and Vande Velde, C. (2019). “RNA granules and their role in neurodegenerative diseases” in *The biology of mRNA: Structure and function*. eds. M. Oeffinger and D. Zenklusen (Cham: Springer International Publishing), 195–245.
- Sirabella, R., Valsecchi, V., Anzilotti, S., Cuomo, O., Vinciguerra, A., Cepparulo, P., et al. (2018). Ionic homeostasis maintenance in ALS: focus on new therapeutic targets. *Front. Neurosci.* 12:510. doi: 10.3389/fnins.2018.00510
- Sommer, D., Rajkumar, S., Seidel, M., Aly, A., Ludolph, A., Ho, R., et al. (2022). Aging-dependent altered transcriptional programs underlie activity impairments in human C9orf72-mutant motor neurons. *Front. Mol. Neurosci.* 15:894230. doi: 10.3389/fnmol.2022.894230
- Sreedharan, J., Blair, I. P., Tripathi, V. B., Hu, X., Vance, C., Rogelj, B., et al. (2008). TDP-43 mutations in familial and sporadic amyotrophic lateral sclerosis. *Science* 319, 1668–1672. doi: 10.1126/science.1154584
- Streit, L., Kuhn, T., Vomhof, T., Bopp, V., Ludolph, A. C., Weishaupt, J. H., et al. (2022). Stress induced TDP-43 mobility loss independent of stress granules. *Nat. Commun.* 13:5480. doi: 10.1038/s41467-022-32939-0
- Strong, M. J., Volkening, K., Hammond, R., Yang, W., Strong, W., Leystra-Lantz, C., et al. (2007). TDP43 is a human low molecular weight neurofilament (hNFL) mRNA-binding protein. *Mol. Cell. Neurosci.* 35, 320–327. doi: 10.1016/j.mcn.2007.03.007
- Suk, T. R., and Rousseaux, M. W. C. (2020). The role of TDP-43 mislocalization in amyotrophic lateral sclerosis. *Mol. Neurodegener.* 15:45. doi: 10.1186/s13024-020-00397-1
- Taylor, A. M., Blurton-Jones, M., Rhee, S. W., Cribbs, D. H., Cotman, C. W., and Jeon, N. L. (2005). A microfluidic culture platform for CNS axonal injury, regeneration and transport. *Nat. Methods* 2, 599–605. doi: 10.1038/nmeth777
- Tollervy, J. R., Curk, T., Rogelj, B., Briese, M., Cereda, M., Kayikci, M., et al. (2011). Characterizing the RNA targets and position-dependent splicing regulation by TDP-43. *Nat. Neurosci.* 14, 452–458. doi: 10.1038/nn.2778
- van Rheenen, W., van der Spek, R. A. A., Bakker, M. K., van Vugt, J., Hop, P. J., Zwamborn, R. A. J., et al. (2021). Common and rare variant association analyses in amyotrophic lateral sclerosis identify 15 risk loci with distinct genetic architectures and neuron-specific biology. *Nat. Genet.* 53, 1636–1648. doi: 10.1038/s41588-021-00973-1
- Vannocci, T., Notario Manzano, R., Beccalli, O., Bettgazzi, B., Grohovaz, F., Cinque, G., et al. (2018). Adding a temporal dimension to the study of Friedreich's ataxia: the effect of frataxin overexpression in a human cell model. *Dis. Model. Mech.* 11:dmm032706. doi: 10.1242/dmm.032706
- Wang, L., Gutmann, D. H., and Roos, R. P. (2011). Astrocyte loss of mutant SOD1 delays ALS disease onset and progression in G85R transgenic mice. *Hum. Mol. Genet.* 20, 286–293. doi: 10.1093/hmg/ddq463
- Watanabe, S., Oiwa, K., Murata, Y., Komine, O., Sobue, A., Endo, F., et al. (2020). ALS-linked TDP-43(M337V) knock-in mice exhibit splicing deregulation without neurodegeneration. *Mol. Brain* 13:8. doi: 10.1186/s13041-020-0550-4
- White, M. A., Kim, E., Duffy, A., Adalbert, R., Phillips, B. U., Peters, O. M., et al. (2018). TDP-43 gains function due to perturbed autoregulation in a Tardbp knock-in mouse model of ALS-FTD. *Nat. Neurosci.* 21, 552–563. doi: 10.1038/s41593-018-0113-5
- Williams, S. R., and Stuart, G. J. (1999). Mechanisms and consequences of action potential burst firing in rat neocortical pyramidal neurons. *J. Physiol.* 521, 467–482. doi: 10.1111/j.1469-7793.1999.00467.x
- Wolozin, B., and Ivanov, P. (2019). Stress granules and neurodegeneration. *Nat. Rev. Neurosci.* 20, 649–666. doi: 10.1038/s41583-019-0222-5
- Wong, C. E., Jin, L. W., Chu, Y. P., Wei, W. Y., Ho, P. C., and Tsai, K. J. (2021). TDP-43 proteinopathy impairs mRNA granule mediated postsynaptic translation and mRNA metabolism. *Theranostics* 11, 330–345. doi: 10.7150/thno.51004